

How stellar feedback simultaneously regulates star formation and drives outflows

Christopher C. Hayward^{1,2,3*} & Philip F. Hopkins²

¹Center for Computational Astrophysics, Flatiron Institute, 162 Fifth Avenue, New York, NY 10010, USA

²TAPIR 350-17, California Institute of Technology, 1200 E. California Boulevard, Pasadena, CA 91125, USA

³Harvard-Smithsonian Center for Astrophysics, 60 Garden Street, Cambridge, MA 02138, USA

Submitted to MNRAS

ABSTRACT

We present an analytic model for how momentum deposition from stellar feedback simultaneously regulates star formation and drives outflows in a turbulent interstellar medium (ISM). Because the ISM is turbulent, a given patch of ISM exhibits sub-patches with a range of surface densities. The high-density patches are ‘pushed’ by feedback, thereby driving turbulence and self-regulating local star formation. Sufficiently low-density patches, however, are accelerated to above the escape velocity before the region can self-adjust and are thus vented as outflows. When the gas fraction is $\gtrsim 0.3$, the ratio of the turbulent velocity dispersion to the circular velocity is sufficiently high that at any given time, of order half of the ISM has surface density less than the critical value and thus can be blown out on a dynamical time. The resulting outflows have a mass-loading factor ($\eta \equiv \dot{M}_{\text{out}}/\dot{M}_*$) that is inversely proportional to the gas fraction times the circular velocity. At low gas fractions, the star formation rate needed for local self-regulation, and corresponding turbulent Mach number, decline rapidly; the ISM is ‘smoother’, and it is actually *more* difficult to drive winds with large mass-loading factors. Crucially, our model predicts that stellar-feedback-driven outflows should be suppressed at $z \lesssim 1$ in $M_* \gtrsim 10^{10} M_\odot$ galaxies. This mechanism allows massive galaxies to exhibit violent outflows at high redshifts and then ‘shut down’ those outflows at late times, thereby enabling the formation of a smooth, extended thin stellar disk. We provide simple fitting functions for η that should be useful for sub-resolution and semi-analytic models.

Key words: cosmology: theory – galaxies: evolution – galaxies: formation – galaxies: ISM – ISM: jets and outflows – methods: analytical.

1 INTRODUCTION

It is widely believed that stellar feedback is crucial for regulating star formation. In the absence of feedback, gas would be completely converted to stars on a free-fall time. In contrast, the actual efficiency is only a few per cent (e.g. Bigiel et al. 2008, 2011; Krumholz et al. 2012; Leroy et al. 2013), although the efficiency per free-fall time can be as high as unity for individual giant molecular clouds (GMCs; Murray 2011). Similarly, without feedback, one would expect most gas in dark matter halos to have been converted into stars by the present day. Thus, the ratio of stellar mass to halo mass should be equal to the baryon fraction (e.g. Cole 1991; White & Frenk 1991; Blanchard et al. 1992; Balogh et al. 2001); however, for all halo masses, the stellar-to-halo mass ratio is much less than this value (e.g. Conroy & Wechsler 2009; Moster et al. 2013; Behroozi et al. 2013). To avoid over-producing stars in numerical simulations and semi-analytic models (SAMs) of galaxy

formation, it is necessary to invoke some form(s) of strong stellar feedback (see Somerville & Davé 2014 for a recent review). It has long been recognised that supernova feedback can generate strong outflows and thus may provide a solution to this overcooling problem (e.g. Mathews & Baker 1971; Larson 1974; Dekel & Silk 1986; White & Rees 1978; White & Frenk 1991). Other potentially important stellar feedback channels include stellar winds, radiation pressure, and photoionization (see Hopkins et al. 2012b and references therein), in addition to cosmic rays (e.g. Uhlig et al. 2012; Hanaaz et al. 2013; Booth et al. 2013; Salem & Bryan 2014; Salem et al. 2014; Girichidis et al. 2016). This feedback stabilizes the interstellar medium (ISM) such that only a few per cent of the gas mass is converted into stars per orbital time and the Kennicutt-Schmidt relation (Schmidt 1959; Kennicutt 1998) can be reproduced (e.g. Stinson et al. 2006; Shetty & Ostriker 2008, 2012; Kim et al. 2011; Ostriker & Shetty 2011; Hopkins et al. 2012b, 2014; Kim et al. 2013; Agertz & Kravtsov 2015a). Moreover, feedback is thought to power strong outflows that prevent most of the gas accreted onto galaxy halos from ever forming stars: for most galaxy

* E-mail: chayward@simonsfoundation.org

masses, the required ‘mass-loading factor’, η , which is the ratio of the mass outflow rate to the star formation rate (SFR), must be significantly greater than unity (e.g. Benson 2014; Lu et al. 2014, 2015; Mitra et al. 2015).

There is an increasing amount of observational evidence for the existence of stellar-feedback-driven outflows (e.g. Lynds & Sandage 1963; Burbidge et al. 1964; Heckman et al. 1990, 2000, 2015; Martin 1996, 1998, 1999, 2005, 2006; Weiner et al. 2009; Steidel et al. 2010; Bordoloi et al. 2011; Martin et al. 2012; Bouché et al. 2012; Diamond-Stanic et al. 2012; Leitherer et al. 2013; Chisholm et al. 2014; see Veilleux et al. 2005 for a review). In principle, observations of outflows may be used to distinguish among outflow models, whether they are prescriptive (i.e. sub-resolution) or predictive. However, inferring the total mass outflow rate is challenging, especially because the outflows are multiphase (e.g. Martin 2005, 2006; Leroy et al. 2015). Moreover, unless direct predictions for line profiles are provided by theorists, it is difficult to ensure that the observational and theoretical definitions of what gas is outflowing are consistent. Thus, it may not be possible to use current observations to distinguish amongst outflow models or provide phenomenological scalings for simulations, but this is certainly a topic that is worthy of further consideration.

Because of resolution limitations, cosmological simulations typically incorporate outflows driven by supernova feedback using sub-resolution models. Some (e.g. Navarro & White 1993; Springel & Hernquist 2003; Oppenheimer & Davé 2006, 2008; Oppenheimer et al. 2010; Dalla Vecchia & Schaye 2008; Schaye et al. 2010; Hirschmann et al. 2013; Vogelsberger et al. 2013; Anglés-Alcázar et al. 2014; Torrey et al. 2014) treat supernova feedback by injecting kinetic energy (i.e. ‘kicks’) into the neighboring gas elements. Many of these implementations kinematically decouple the outflow particles to ensure that they escape the ISM. The other commonly used technique is the ‘blastwave’ model, in which thermal energy is injected into the ISM surrounding supernova particles (e.g. Katz et al. 1996; Thacker & Couchman 2000; Stinson et al. 2006, 2013; Governato et al. 2007, 2010, 2012; Dubois & Teyssier 2008; Bournaud et al. 2010). However, because young star particles are typically located in regions of dense gas, where the cooling time is short, such feedback is ineffective because the supernova feedback energy is rapidly radiated away. To overcome this problem, it is common to either artificially disable cooling for some fixed time interval (e.g. Stinson et al. 2006, 2013) or store the supernova feedback energy until it is guaranteed to generate a blastwave, albeit on artificially large (but numerically resolved) scales (e.g. Dalla Vecchia & Schaye 2012; Crain et al. 2015; Schaye et al. 2015).

Such treatments of outflows are useful because they enable these simulations to satisfy a wide variety of observational constraints (e.g. Oppenheimer & Davé 2006, 2008; Oppenheimer et al. 2010, 2012; Davé et al. 2011a,b, 2013; Puchwein & Springel 2013; Vogelsberger et al. 2014; Schaye et al. 2015; Ford et al. 2015), although some significant discrepancies between the results of state-of-the-art cosmological simulations and models remain (see Vogelsberger et al. 2014, Genel et al. 2014, and Schaye et al. 2015 for discussions). Similarly, SAMs must include strong outflows to match observational constraints such as the galaxy stellar mass function (e.g. Somerville & Primack 1999; Somerville et al. 2008; Benson et al. 2003; Benson 2014; Croton et al. 2006; Guo et al. 2011, 2013; Lu et al. 2014). Comparisons with observations of the circumgalactic and intergalactic media (e.g. Oppenheimer & Davé 2009; Oppenheimer et al. 2012; Davé et al. 2010; Ford et al. 2013, 2014, 2015) and X-ray observations (e.g. Cox et al. 2006; Le Brun et al. 2014; Zhang et al. 2014; Bogdán et al. 2015; Schaye et al.

2015) can be used to constrain outflow models. However, because of their manner of implementation and required tuning, these outflow models cannot be considered predictive, and it is highly desirable to develop a *physical, predictive* model for how stellar feedback drives outflows.

In SAMs (e.g. Croton et al. 2006; Somerville et al. 2008; Guo et al. 2011, 2013; White et al. 2015) and cosmological simulations (Okamoto et al. 2010; Vogelsberger et al. 2013; Torrey et al. 2014; cf. e.g. Oppenheimer & Davé 2008; Schaye et al. 2015), it is common to assume that the outflow mass-loading factor η scales with the halo circular velocity (see Somerville & Davé 2014 for additional discussion). Thus, at fixed halo mass (and thus approximately constant stellar mass because the redshift evolution in the stellar mass–halo mass relation is weak; Behroozi et al. 2013), the mass-loading factor decreases with increasing redshift. For Milky Way-mass galaxies, this effect inevitably leads to too much high-redshift star formation or over-suppression of low-redshift star formation, depending on the assumed normalisation of the $\eta - v_c$ relation (e.g. Torrey et al. 2014; White et al. 2015). Moreover, observational constraints require that the mass-loading factor at fixed stellar mass *increases* with increasing redshift (Mitra et al. 2015); this trend cannot be reproduced in models that assume simple $\eta \propto v_c^{-1}$ or $\eta \propto v_c^{-2}$ scalings. An alternative method for calculating the mass-loading factor is thus required.

Recently, multiple groups have made significant advances by generating outflows self-consistently via stellar feedback without resorting to delayed cooling or kinematic decoupling (Hopkins et al. 2012a, 2013, 2014; Agertz et al. 2013; Agertz & Kravtsov 2015a,b). In particular, Muratov et al. (2015) have demonstrated that stellar feedback can effectively drive outflows in galaxies of stellar mass $M_\star \lesssim 10^{10} M_\odot$ at all redshifts. The simulated galaxies agree well with observational constraints, such as the stellar mass–halo mass, Kennicutt–Schmidt, and SFR–stellar mass relations (Hopkins et al. 2014). The *predicted* mass-loading factors are considerably less than typically assumed in large-volume cosmological simulations and SAMs, which suggests that the latter use outflow models that are inconsistent with the scalings of Muratov et al. (2015) or/and they must invoke higher mass-loading factors to compensate for limitations of the (sub-resolution) feedback models employed. Moreover, Muratov et al. (2015) noted that outflows were significantly suppressed in their simulated galaxies with $M_\star \gtrsim 10^{10} M_\odot$ at low redshift ($z \lesssim 1$). This suppression of outflows enables these massive galaxies to transition from highly turbulent, clumpy discs characterised by bursts of star formation and subsequent outflows to well-ordered, thin, steadily star-forming disc galaxies at $z = 0$.

The aforementioned simulations have the advantage of including stellar feedback in an explicit, resolved manner and generating outflows self-consistently. However, it can be difficult to extract physical explanations for phenomena ‘observed’ in such simulations because of the complexity of the simulations. For this reason, Muratov et al. (2015) did not identify the physical origin of the suppression of outflows in their simulated $M_\star \gtrsim 10^{10} M_\odot$ galaxies at $z \lesssim 1$. Simple analytic models are a useful complementary tool that can be used to posit potential physical mechanisms, the veracity of which can be checked via detailed simulations and, ideally, comparisons with observations. In this work, we present an analytic theory for stellar-feedback-driven galactic outflows. One of the most interesting features of the model is that, as we will discuss in detail below, it predicts suppression of outflows in massive galaxies at low redshift that is qualitatively consistent with the

simulation-based results of [Muratov et al. \(2015\)](#). Consequently, our model may offer a physical explanation for those results.

This work builds upon a number of previous works. The first key assumption of our model is that star formation is self-regulated. By this, we mean that momentum deposition from stellar feedback or photo-heating from star formation is assumed to provide vertical pressure support against gravity such that a galaxy maintains a quasi-equilibrium state. Under this assumption, the rate of momentum or energy deposition sets the star formation rate. Various previous works have presented such models (e.g. [Murray et al. 2005, 2011](#); [Thompson et al. 2005](#); [Ostriker et al. 2010](#); [Ostriker & Shetty 2011](#); [Shetty & Ostriker 2012](#); [Faucher-Giguère et al. 2013](#)). In particular, we rely heavily on the work of [Faucher-Giguère et al. \(2013, hereafter FQH13\)](#).

The second key assumption is that the gas that will be blown out by stellar feedback corresponds to the gas that can be accelerated to the local escape velocity before the density distribution is reset by turbulence. As we demonstrate below, this implies that gas below some maximum surface density will be blown out. Because the ISM is turbulent, a given ‘macroscopic’ patch of ISM exhibits sub-patches with a range of surface densities. [Thompson & Krumholz \(2016, hereafter TK14\)](#) demonstrated that this property of supersonic turbulence implies that even when a galaxy is globally below the Eddington limit (i.e. the surface density above which radiation pressure on dust provides the dominant pressure support against gravity; [Scoville 2003](#); [Thompson et al. 2005](#)), it will have sub-patches that are super-Eddington. As noted by TK14, virtually all previous models for how momentum deposition drives turbulence (e.g. [Krumholz & McKee 2005](#); [Krumholz et al. 2009b](#); [Murray et al. 2010](#); [Ostriker & Shetty 2011](#); FQH13) and generates outflows (e.g. [Murray et al. 2005, 2011](#); [Thompson et al. 2005](#)) have considered only the mean gas surface density. We build upon the work of TK14 by applying an analysis similar to theirs to a self-regulated galaxy formation model. Specifically, we use the results of FQH13 for the high-surface-density regime, in which turbulent pressure dominates. For the low-surface-density regime, in which thermal pressure dominates, we calculate the quasi-equilibrium SFR surface density relation (see [Ostriker et al. 2010](#) for a more detailed treatment). Through this synthesis, we predict the mass-loading factor of stellar-feedback-driven outflows as a function of galaxy properties.

The remainder of this work is organised as follows: [Section 2](#) presents our method for calculating the mass outflow rate for momentum-driven outflows in a turbulent ISM. [Section 3](#) derives expressions for the mass-loading factor in the regime in which a galaxy/patch is supported by turbulent pressure, whereas [Section 4](#) considers the regime in which thermal pressure balances gravity. In [Section 5](#), we use empirically based scalings to demonstrate how the mass-loading factor depends on stellar mass and redshift. [Section 6](#) presents some implications of our model for galaxy evolution, and [Section 7](#) outlines how one could implement our model in hydrodynamical simulations or SAMs. We summarize our conclusions in [Section 8](#). In [Appendix A](#), we derive the equilibrium SFR surface density and mass-loading factor relations for the thermal pressure-dominated regime. [Appendix B](#) presents the empirically based scaling relations that we use to determine the dependence of the mass-loading factor on stellar mass and redshift in [Section 5](#). In [Appendix C](#), we use these relations to determine which regime is relevant as a function of mass and redshift.

2 HOW STELLAR FEEDBACK DRIVES OUTFLOWS IN A TURBULENT ISM

In this section, we present our approach for calculating the mass outflow rate of an outflow driven by momentum deposition from stellar feedback. Crucially, we consider a turbulent ISM in which a patch/disc¹ of some mean gas surface density contains sub-patches with a range of gas surface densities.² We first present our criterion for determining which gas will be blown out on a coherence time (i.e. before turbulence ‘resets’ the density distribution), and we then discuss how we calculate the fraction of the ISM mass that satisfies this criterion.

2.1 Which gas can be blown out?

As noted by TK14, in a turbulent ISM, a given patch of ISM with mean gas surface density $\langle \Sigma_g \rangle$ will contain sub-patches with a range of surface densities. For a sub-patch of ISM with gas surface density Σ_g to be expelled, we assume that it must be accelerated to the escape velocity of the disc, v_{esc} , within a coherence time. The motivation for this assumption is that over a coherence time, turbulence will ‘reset’ the gas surface density distribution of the disc; for patches with surface density initially less than the mean surface density, this will tend to cause the surface density below the patch to increase, and this high-surface-density gas will ‘block’ further momentum injection from local stellar feedback. Consequently, the patch will no longer be accelerated and will rain back down onto the disc rather than be expelled as an outflow. However, this assumption may not hold because driving outflows may be a relatively slow process that is the result of several acceleration steps (e.g. [Hill et al. 2012](#); [Girichidis et al. 2016](#)). Local stellar feedback from e.g. supernovae may push a patch to some height above the disc but not accelerate it to the escape velocity. Then, other sources of acceleration, such as supernovae from runaway OB stars (e.g. [Li et al. 2015](#)) or cosmic rays ([Uhlig et al. 2012](#); [Booth et al. 2013](#); [Hanasz et al. 2013](#); [Salem & Bryan 2014](#); [Salem et al. 2014](#); [Girichidis et al. 2016](#)), may provide the remaining momentum deposition necessary to accelerate the patch to the escape velocity. In principle, we could crudely account for such multi-step acceleration in our model by requiring the gas to be accelerated only to some fraction of the escape velocity. However, given the poorly understood nature of the above processes and considerations of simplicity, we will not do so in the present work.

With the above caveats in mind, to make the problem tractable, we will assume that a sub-patch of ISM must be accelerated to the escape velocity within a coherence time, and we recognise that this assumption may require revision in future work. In turbulence, the coherence time is $\sim t_{\text{eddy}} \sim \sigma_{\text{eddy}}/l_{\text{eddy}}$, where t_{eddy} and σ_{eddy} are the characteristic timescale and turbulent velocity associated with eddies on a spatial scale l_{eddy} . In a vertically stratified, supersonically turbulent disc with scaleheight h , vertical force balance

¹ We will use the terms ‘patch’ and ‘disc’ interchangeably because the model can be applied to either an entire galaxy, using galaxy-averaged quantities, or sub-regions of galaxies, as long as the latter are of a size greater than the disc scaleheight.

² Because we are considering both the mean gas surface density of a patch and the surface densities of sub-patches, we distinguish the former using the notation $\langle \Sigma_g \rangle$. All other quantities, such as the equilibrium SFR surface density, correspond to averages over the total patch/disc. For simplicity of notation, we omit the angle brackets for all spatially averaged quantities except $\langle \Sigma_g \rangle$.

requires that the largest eddies have scaleheight $\sim h \sim \sigma_T/\Omega$, where Ω is the local orbital frequency and σ_T is the characteristic turbulent velocity of the medium for eddies with $l_{\text{eddy}} \sim h$. Since Σ_g is the gas volume density integrated in the vertical direction, we are considering *only* patches integrated through the disc (i.e. with minimum individual size $\sim h$). Moreover, because the large scales contain all the power in density fluctuations, we are primarily concerned with eddies with $l_{\text{eddy}} \sim h$. Thus, we obtain the typical coherence time $\sim \Omega^{-1}$, and we therefore require

$$\dot{P}\Omega^{-1} > mv_{\text{esc}}, \quad (1)$$

where \dot{P} is the momentum deposition rate and m is the mass of the patch of ISM. For a disc in radial centrifugal balance in an isothermal potential with circular velocity $v_{\text{c,gal}}$, the total mass enclosed with radius r is $M(r) = v_{\text{c,gal}}^2 r/G$. The escape velocity is $v_{\text{esc}} = \sqrt{GM(r)/r} = \sqrt{2}v_{\text{c,gal}}$. Thus,

$$\dot{P} \gtrsim \sqrt{2}\Omega m v_{\text{c,gal}}. \quad (2)$$

In terms of surface density,

$$\dot{\Sigma}_P \gtrsim \sqrt{2}\Omega \Sigma_g v_{\text{c,gal}}, \quad (3)$$

where $\dot{\Sigma}_P$ is the momentum deposition rate per unit area.

For sources of stellar feedback such as winds, supernovae, and radiation pressure, the momentum deposition rate per unit area is given by

$$\dot{\Sigma}_P = \left(\frac{P_\star}{m_\star}\right) \dot{\Sigma}_\star, \quad (4)$$

where $\dot{\Sigma}_\star$ is the mean SFR surface density of the patch and (P_\star/m_\star) is the momentum deposited per unit stellar mass formed. This value varies depending on the source of stellar feedback being considered. Following FQH13, we will use $(P_\star/m_\star) = 3000 \text{ km s}^{-1}$, which is appropriate for supernova feedback (see FQH13 and references therein), as our fiducial value. We will retain this factor such that our results can be generalized for other sources of stellar feedback.

Thus, the surface density below which gas will be accelerated to the escape velocity on a coherence time and thus blown out is

$$\Sigma_g^{\text{max}} \equiv \left(\frac{P_\star}{m_\star}\right) \frac{\dot{\Sigma}_\star}{\sqrt{2}\Omega v_{\text{c,gal}}}. \quad (5)$$

The above framework assumes that the outflows are momentum-driven. The fiducial value $P_\star/m_\star = 3000 \text{ km s}^{-1}$ is based on the assumption that SN remnants go through the energy-conserving Sedov-Taylor (Taylor 1950; Sedov 1959) phase in which energy is converted into momentum. The reason that the outflows can be considered momentum-driven is that we assume that by the time the outflows ‘break out’ of the disc, the energy-conserving phase has ended (see FQH13 for details). This assumption is justified as long as the cooling radii of the supernova ejecta are less than the disc scaleheight. If this condition does not hold (i.e. a supernova remnant expands to of order the disc scaleheight or greater while still in the Sedov-Taylor phase), the outflows should be treated as energy-conserving. We can estimate when this assumption will be violated as follows. The cooling radius for an individual supernova remnant is $R_{\text{cool}} \sim 14 \text{ pc}(n/\text{cm}^{-3})^{-3/7}$ (Cioffi et al. 1988; Thornton et al. 1998), where n is the number density of the ambient medium; we have ignored the weak metallicity dependence. The disc scaleheight is $h \sim c_s/\Omega$, where c_s is

the sound speed.³ Using the relation $n \sim \langle \Sigma_g \rangle / 2m_p h$, where m_p is the proton mass, the cooling radius can be expressed as

$$R_{\text{cool}} \sim 14 \text{ pc} \left(\frac{\langle \Sigma_g \rangle / 2m_p h}{1 \text{ cm}^{-3}} \right)^{-3/7}. \quad (6)$$

The cooling radius is greater than the disc scaleheight, $R_{\text{cool}} \gtrsim h$, when

$$\langle \Sigma_g \rangle \lesssim 1 \text{ M}_\odot \text{ pc}^{-2} \left(\frac{h}{14 \text{ pc}} \right)^{-4/3}. \quad (7)$$

Thus, we expect energetically driven outflows to be significant only when the local gas surface density (i.e. the gas surface density averaged over the cooling radius) is $\lesssim 1 \text{ M}_\odot \text{ pc}^{-2}$. Because patches with such low surface density will almost always be below our calculated critical surface density, we will include this material in the outflowing material, and the actual driving method is irrelevant for the purposes of calculating the outflow fraction.

It is certainly possible for this condition to be satisfied in the outer regions of discs or if the surface density of the local ISM has already been reduced considerably by other forms of feedback or other supernovae before a supernova explodes (e.g. Larson 1974; Cantó et al. 2000; Wada & Norman 2001; Martizzi et al. 2015). Still, even if it is possible for supernova ejecta to escape the galaxy while still in the energy-conserving phase, the expected mass loading factor is small because little material will be entrained; thus, the amount of outflowing gas will be of order the supernova ejecta mass. For standard initial mass functions, on average, each supernova ejects of order 10 M_\odot , and there is approximately one supernova per 100 M_\odot formed (Kroupa 2001; Chabrier 2003). Thus, we expect the mass-loading factor to be $\lesssim 0.1$, and indeed, numerical simulations of energy-driven outflows from supernovae suggest that very little mass is blown out (e.g. Mac Low & Ferrara 1999; Strickland & Stevens 2000). For this reason, we neglect this form of feedback in the current work.

2.2 What fraction of the ISM will be blown out?

We now calculate the fraction of the ISM with $\Sigma_g < \Sigma_g^{\text{max}}$ by considering the distribution of gas surface density in a turbulent ISM, closely following the analysis of TK14. For supersonic isothermal turbulence, the probability distribution functions (PDFs) of both the volume and surface densities are approximately lognormal (e.g. Ostriker et al. 2001; Vázquez-Semadeni & García 2001; Federrath et al. 2010; Konstantin et al. 2012a,b, 2015). Given a value of Σ_g^{max} , we can use the gas density PDF to calculate the mass fraction of the gas that is blown out by stellar-feedback-driven outflows, f_{out} , which we refer to as the ‘outflow fraction’, by computing the mass fraction of the disc that has $\Sigma_g < \Sigma_g^{\text{max}}$. This can be done by combining equations (8), (12) and (14) of TK14. Define

$$x_{\text{out}} \equiv \ln \left(\frac{\Sigma_g^{\text{max}}}{\langle \Sigma_g \rangle} \right). \quad (8)$$

Then, from equation (8) of TK14, the outflow fraction is

$$f_{\text{out}} = \int_{-\infty}^{x_{\text{out}}} p_-(x) dx = \frac{1}{2} \left[1 - \text{erf} \left(\frac{-2x_{\text{out}} + \sigma_{\ln \Sigma_g}^2}{2\sqrt{2}\sigma_{\ln \Sigma_g}} \right) \right], \quad (9)$$

³ This expression for the disc scaleheight assumes that the disc is supported by thermal rather than turbulent pressure. Below, we shall see that this is the case for the relevant surface densities.

where erf denotes the error function and $\sigma_{\ln \Sigma_g}$ is the dispersion of the logarithm of the gas surface density. Note that we have used $p_-(x)$ because we wish to calculate the fraction of the mass (rather than the area) that has $\Sigma_g < \Sigma_g^{\max}$; see TK14 for details. The width of the PDF of the logarithm of the gas surface density is (equation 12 of TK14)

$$\sigma_{\ln \Sigma_g}^2 \approx (1 + R\mathcal{M}^2/4), \quad (10)$$

where $\mathcal{M} \equiv \sigma_T/c_s$ is the Mach number of the turbulence and R is given by equation (14) of TK14,

$$R = \frac{1}{2} \left(\frac{3 - \alpha}{2 - \alpha} \right) \left[\frac{1 - \mathcal{M}^{2(2-\alpha)}}{1 - \mathcal{M}^{2(3-\alpha)}} \right]. \quad (11)$$

Following TK14, we assume that the power-law index of the power spectrum of the turbulence is $\alpha = 2.5$ because in the turbulent-pressure-supported regime, the turbulence is generally highly supersonic. When our model predicts that the turbulence is transonic, we instead use $\alpha = 3.7$. However, our results are insensitive to the exact value of α used. The above equations can be used to calculate f_{out} if \mathcal{M} and Σ_g^{\max} are known.

The primary quantity with which we are concerned in this work is the mass-loading factor, $\eta \equiv \dot{M}_{\text{out}}/\dot{M}_* = \dot{\Sigma}_{\text{out}}/\dot{\Sigma}_*$, where \dot{M}_{out} is the mass outflow rate and $\dot{\Sigma}_{\text{out}}$ is the mass outflow rate per unit area, which is $\dot{\Sigma}_{\text{out}} = f_{\text{out}}\langle\Sigma_g\rangle\Omega$ by construction in our model. Thus, the mass-loading factor is

$$\eta = \frac{f_{\text{out}}\langle\Sigma_g\rangle\Omega}{\dot{\Sigma}_*}. \quad (12)$$

3 TURBULENT PRESSURE-SUPPORTED REGIME

Now that we have presented the formalism for calculating the mass outflow rate, we must determine the equilibrium SFR surface density relations. We first consider the limit in which turbulent pressure is the dominant source of pressure support against gravity. This regime is studied in detail in FQH13 (see also Thompson et al. 2005 and Ostriker & Shetty 2011), so we will only summarise the model here. Stellar feedback injects momentum into the ISM. A fraction f_{out} drives outflows, whereas the remaining $(1 - f_{\text{out}})$ pushes on gas that will not be blown out and drives turbulence with a momentum injection rate per unit area of $(1 - f_{\text{out}})\dot{\Sigma}_*(P_*/m_*)$. We have included the $(1 - f_{\text{out}})$ factor so that we do not double-count the momentum that drives outflows rather than stirring the gas. As argued above, turbulence dissipates energy on a crossing time, Ω^{-1} . In equilibrium, the momentum injection rate per unit area must equal the dissipation rate per unit area, $\sim (1 - f_{\text{out}})\langle\Sigma_g\rangle\sigma_T\Omega$. We also include the $(1 - f_{\text{out}})$ factor here because we must balance the dissipation only in the gas that remains in the disc, not the outflowing material. Setting the momentum injection and dissipation rates equal, we have

$$\dot{\Sigma}_* \approx \left(\frac{P_*}{m_*} \right)^{-1} \sigma_T \Omega \langle\Sigma_g\rangle. \quad (13)$$

The Toomre (1964) Q parameter is

$$Q = \frac{\kappa \sqrt{c_s^2 + \sigma_T^2}}{\pi G \langle\Sigma_g\rangle}, \quad (14)$$

where $\kappa \sim \sqrt{2}\Omega$ is the epicyclic frequency, c_s is the sound speed, σ_T is the turbulent velocity dispersion and $\langle\Sigma_g\rangle$ is the mean gas surface density of the patch/disc. We assume that turbulence provides the dominant vertical pressure support against gravity; thus,

$\sqrt{c_s^2 + \sigma_T^2} \sim \sigma_T$. We can use the Toomre Q to rewrite equation (13) in the following form:

$$\dot{\Sigma}_* \approx \frac{\pi G Q}{\sqrt{2}} \left(\frac{P_*}{m_*} \right)^{-1} \langle\Sigma_g\rangle^2. \quad (15)$$

FQH13 present a somewhat more sophisticated derivation of the equilibrium SFR surface density relation in this regime. Their expression has the same dependences on $\langle\Sigma_g\rangle$, Q and (P_*/m_*) , but the prefactor differs. Below, we will use the expression derived by FQH13 (their equation 18):

$$\dot{\Sigma}_*^{\text{turb}} = \frac{2\sqrt{2}\pi G Q \phi}{\mathcal{F}'} \left(\frac{P_*}{m_*} \right)^{-1} \langle\Sigma_g\rangle^2, \quad (16)$$

where G is the gravitational constant, Q is the Toomre Q parameter, ϕ is an order-unity parameter that is ~ 1 for a thin disc in a spherical potential and $\sim 1/Q$ for a self-gravitating pure gas disc, and \mathcal{F}' is a dimensionless parameter that encapsulates uncertain factors that are of order unity (see Thompson et al. 2005 and Ostriker & Shetty 2011 for similar expressions).⁴ We have compared this equilibrium SFR surface density relation with the results of high-resolution galaxy simulations that include resolved stellar feedback and found excellent agreement (see also Kim et al. 2013).

Given the equilibrium SFR surface density, we can predict how the outflow fraction depends on galaxy properties. Combining equations (5) and (16), we find that in this regime, the critical surface density below which gas can be blown out on a coherence time is

$$\Sigma_g^{\max} = \frac{2\pi G Q \phi}{\mathcal{F}' \Omega v_{c,\text{gal}}} \langle\Sigma_g\rangle^2 \equiv \Sigma_{g,\text{turb}}^{\max}. \quad (17)$$

We can express $\Sigma_{g,\text{turb}}^{\max}$ in a more useful form as follows. Using the definition of the Toomre Q (equation 14) and $\sigma_T^2 \gg c_s^2$ (because we are considering the limit in which turbulence dominates the pressure support), we have

$$\frac{\langle\Sigma_g\rangle}{\Omega} \sim \frac{\sqrt{2}\sigma_T}{\pi G Q_{\text{turb}}}, \quad (18)$$

where Q_{turb} denotes the turbulent Toomre Q (i.e. equation 14 with $c_s = 0$). Using equation (18), equation (17) can be rewritten as

$$\Sigma_{g,\text{turb}}^{\max} = \frac{2\sqrt{2}\pi\phi}{\mathcal{F}'} \frac{\sigma_T}{v_{c,\text{gal}}} \langle\Sigma_g\rangle. \quad (19)$$

For a turbulent-pressure-supported disc (equation 9 of FQH13),

$$\frac{\sigma_T}{v_{c,\text{gal}}} = \frac{Q_{\text{turb}}}{\sqrt{2}} f_g, \quad (20)$$

where we have used $v_{c,\text{gal}} = \sqrt{2}\sigma$, in which σ is the velocity dispersion of the isothermal potential. In the above equation, $f_g \equiv M_g/(M_g + M_*)$ is the gas fraction of the disc/patch; note that $f_g \leq 1$ by definition. Combining equations (19) and (20), we have

$$\Sigma_{g,\text{turb}}^{\max} = \frac{2\phi Q_{\text{turb}}}{\mathcal{F}'} f_g \langle\Sigma_g\rangle \quad (21)$$

⁴ In their equation (18), FQH13 include the term $(1 - f_w)$, where f_w is the fraction of the input momentum that drives outflows (rather than supports the disc against gravity); this is equivalent to our f_{out} . However, as we note above, the outflowing gas does not need to be supported against gravity; thus, there should be a $(1 - f_w)$ factor on the right-hand side of their equation (14), which would eliminate the $(1 - f_w)$ term in their equation (18). Consequently, we use the prefactor $\mathcal{F}' = f_P f_h \gamma$, where f_P , f_h , and γ are order-unity coefficients that encapsulate various uncertainties (see FQH13 for details), and we note that this factor does not include the $(1 - f_w)$ term.

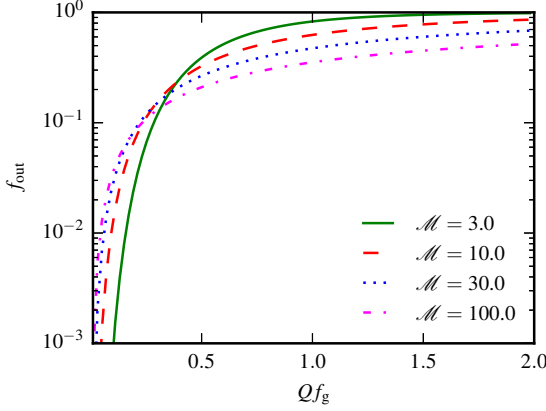


Figure 1. The fraction of the ISM mass that will be blown out on a coherence time, $f_{\text{out}}^{\text{turb}}$, versus the product of the turbulent Toomre Q and the gas fraction, $Q_{\text{turb}}f_g (= \sqrt{2}\sigma_T/v_{c,\text{gal}})$, for different Mach numbers (see the legend); we assume that the order-unity parameters ϕ and \mathcal{F}' are exactly unity. There is a critical $Q_{\text{turb}}f_g$ value below which $f_{\text{out}}^{\text{turb}}$ decreases exponentially because for low $Q_{\text{turb}}f_g$, the rms turbulent velocity is much less than the escape velocity. Thus, only extremely low-surface-density patches, which lie outside of the ‘core’ of the lognormal distribution, can be blown out (because the momentum deposition rate depends on the *mean* SFR and thus gas surface density, whereas the amount of momentum required to accelerate a patch to the escape velocity depends on the *local* gas surface density). When $Q_{\text{turb}}f_g$ is large, the rms turbulent velocity is sufficiently high that patches with surface densities of order the mean surface density can be blown out, and the outflow fraction becomes of order unity.

$$= \frac{2\sqrt{2}\phi}{\mathcal{F}'} \left(\frac{\sigma_T}{v_{c,\text{gal}}} \right) \langle \Sigma_g \rangle. \quad (22)$$

Thus,

$$x_{\text{out}}^{\text{turb}} = \ln \left(\frac{2\phi Q_{\text{turb}}f_g}{\mathcal{F}'} \right) \quad (23)$$

$$= \ln \left[\frac{2\sqrt{2}\phi}{\mathcal{F}'} \left(\frac{\sigma_T}{v_{c,\text{gal}}} \right) \right]. \quad (24)$$

To calculate the Mach number, we require the sound speed,

$$c_s = \sqrt{\frac{k_B T}{\mu}}, \quad (25)$$

where $\mu \approx 0.6$ amu for a fully ionized plasma of primordial composition. Thus, for $T = 10^4$ K, $c_s \approx 12$ km s⁻¹. Equations (20) and (25) imply

$$\mathcal{M} = \frac{Q_{\text{turb}}f_g v_{c,\text{gal}}}{\sqrt{2k_B T/\mu}} \equiv \mathcal{M}_{\text{turb}} \quad (26)$$

$$\approx 6Q_{\text{turb}} \left(\frac{\mu}{0.6} \right)^{1/2} \left(\frac{T}{10^4 \text{ K}} \right)^{-1/2} \left(\frac{f_g v_{c,\text{gal}}}{100 \text{ km s}^{-1}} \right). \quad (27)$$

We assume that the diffuse, turbulence-supported ISM has a temperature of $\sim 10^4$ K.⁵

⁵ For $T = 10^4$ K, equation (26) yields $\mathcal{M} < 1$ for $f_g v_{c,\text{gal}} < 17$ km s⁻¹. However, gas cooling onto galaxies of this circular velocity should be suppressed by photoionisation from the metagalactic ultraviolet background (Thoul & Weinberg 1996; Bullock et al. 2000; Hoefft et al. 2006; Okamoto et al. 2008). Thus, galaxies with $v_{c,\text{gal}} \lesssim 20$ km s⁻¹ (equivalent to $M_\star \lesssim 10^6 M_\odot$) are not considered in detail in this work.

Fig. 1 shows the outflow fraction (f_{out} , i.e. the solution to equation 9) versus $Q_{\text{turb}}f_g$ for various Mach numbers (see the legend). f_{out} increases with $Q_{\text{turb}}f_g = \sqrt{2}\sigma_T/v_{c,\text{gal}}$ because the ratio $\Sigma_g^{\text{max}}/\langle \Sigma_g \rangle \propto Q_{\text{turb}}f_g$. Moreover, there is a sharp cutoff at $Q_{\text{turb}}f_g \sim 0.3$; this cutoff occurs at lower $Q_{\text{turb}}f_g$ values for higher Mach numbers because the lognormal gas surface density PDF broadens as the Mach number is increased (see below for details). The reason for this behavior is as follows: $\Sigma_{g,\text{turb}}^{\text{max}}$, the surface density below which gas is blown out, scales as Σ_\star (equation 5), which scales as $Q_{\text{turb}}\langle \Sigma_g \rangle^2$ (equation 16). Thus, the ratio $\Sigma_{g,\text{turb}}^{\text{max}}/\langle \Sigma_g \rangle \propto Q_{\text{turb}}\langle \Sigma_g \rangle$. As $Q_{\text{turb}}f_g$ decreases, $Q_{\text{turb}}\langle \Sigma_g \rangle$ decreases, and thus $\Sigma_{g,\text{turb}}^{\text{max}}/\langle \Sigma_g \rangle$ decreases. Consequently, increasingly less of the density PDF is sampled as f_g decreases, and thus f_{out} decreases (see equation 9).⁶ The cutoff occurs when $\Sigma_{g,\text{turb}}^{\text{max}}/\langle \Sigma_g \rangle$ is sufficiently small that only the low-surface-density tail of the lognormal PDF is sampled.

Put more physically, when $Q_{\text{turb}}f_g$ is low, the rms turbulent velocity is much less than the escape velocity. The amount of momentum deposited into a patch on a coherence time, and thus the rms turbulent velocity, depends on the *mean* SFR and thus gas surface density. In contrast, the amount of momentum required to accelerate a patch to the escape velocity on a coherence time depends on the *local* gas surface density (i.e. for a fixed amount of momentum, the typical velocity to which gas is accelerated decreases as the mass of gas being pushed is increased). Thus, when the rms turbulent velocity is much less than the escape velocity, only extremely low-surface-density patches (relative to the mean surface density) can be accelerated to the escape velocity. As $Q_{\text{turb}}f_g$ is increased, the rms turbulent velocity becomes comparable to the escape velocity. In this case, patches with surface densities of order the mean surface density can be accelerated to the escape velocity, and the outflow fraction becomes of order unity.

The dependence of the outflow fraction on the Mach number of the turbulence, $\mathcal{M}_{\text{turb}}$, evident in Fig. 1 is also of interest. As the Mach number is increased, the lognormal PDF broadens (see fig. 1 of TK14): the tails contain an increased fraction of the ISM mass, and the core of the distribution contains less (i.e. the fraction of the ISM with surface density near the mean decreases). Consequently, when the critical surface density is in the low-surface-density tail of the lognormal distribution ($Q_{\text{turb}}f_g \lesssim 0.5$ because when $Q_{\text{turb}}f_g = 0.5$, $\Sigma_g^{\text{max}} = \langle \Sigma_g \rangle$), increasing the Mach number increases the outflow fraction. Conversely, when the critical surface density is of order the mean surface density (i.e. the rms turbulent velocity is of order the escape velocity), the outflow fraction decreases with increasing Mach number because an increased fraction of the mass has surface density significantly greater than the mean and thus cannot be blown out.

We have determined the critical surface density below which gas can be blown out on a coherence time. We are thus now in a position to calculate the mass-loading factor, η (equation 12). For clarity, we use the notation η_{turb} to remind the reader that the below expressions apply in the turbulent-pressure-supported regime. Using the equilibrium SFR surface density relation for this regime (equation 16), we have

$$\eta_{\text{turb}} = \frac{\mathcal{F}'}{2\sqrt{2}\pi G Q_{\text{turb}}\phi} f_{\text{out}} \left(\frac{P_\star}{m_\star} \right) \Omega \langle \Sigma_g \rangle^{-1} \quad (28)$$

⁶ Note that f_{out} will increase with increasing $\langle \Sigma_g \rangle$ as long as Σ_\star depends super-linearly on $\langle \Sigma_g \rangle$.

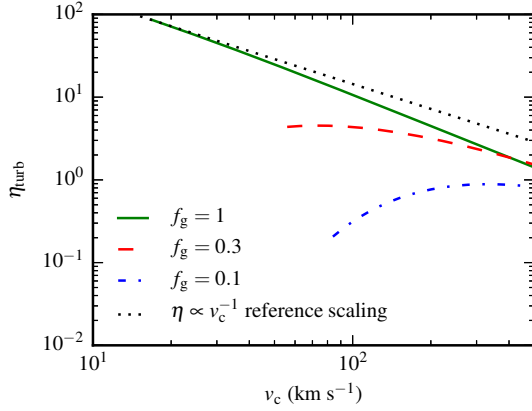


Figure 2. The mass-loading factor (η_{turb}), in the turbulent-pressure-supported regime versus the galaxy circular velocity ($v_{\text{c,gal}}$) for different values of the gas fraction (see the legend). The reference scaling for a momentum-driven outflow, $\eta_{\text{turb}} \propto v_{\text{c,gal}}^{-1}$ (with arbitrary normalization), is indicated by the black dotted line. When the gas fraction is high, η_{turb} decreases slightly more steeply with $v_{\text{c,gal}}$ than the $v_{\text{c,gal}}^{-1}$ reference scaling because $f_{\text{out}}^{\text{turb}}$ (not shown) decreases mildly with $v_{\text{c,gal}}$. When the gas fraction is near or below the critical value of ~ 0.3 , η_{turb} is suppressed considerably. The suppression is stronger at lower $v_{\text{c,gal}}$ values because when $\Sigma_{\text{g}}^{\text{max}}$, the critical surface density below which gas will be blown out on a coherence time, is in the low-surface-density tail of the PDF, the outflow fraction, f_{out} , depends very sensitively on the Mach number, \mathcal{M} (see Fig. 1). For fixed f_{g} , lower $v_{\text{c,gal}}$ results in lower \mathcal{M} and thus significantly lower f_{out} . (N.B. The red dashed and blue dot-dashed lines are truncated at the $v_{\text{c,gal}}$ values at which $\mathcal{M} = 1$ because galaxies with lower $v_{\text{c,gal}}$ values would be supported by thermal, not turbulent, pressure.)

$$\approx 80 \frac{\mathcal{F}'}{Q_{\text{turb}} \phi} f_{\text{out}} \left(\frac{P_{\star}/m_{\star}}{3000 \text{ km s}^{-1}} \right) \times \left(\frac{\Omega}{10 \text{ Gyr}^{-1}} \right) \left(\frac{\langle \Sigma_{\text{g}} \rangle}{10^3 \text{ M}_{\odot} \text{ pc}^{-2}} \right)^{-1}. \quad (29)$$

Equation (28) can be recast into another useful form using equation (18):

$$\eta_{\text{turb}} = \frac{\mathcal{F}'}{2\sqrt{2}\phi} f_{\text{out}} \left(\frac{P_{\star}}{m_{\star}} \right) \sigma_{\text{T}}^{-1} \quad (30)$$

$$\approx 10^2 \frac{\mathcal{F}'}{\phi} f_{\text{out}} \left(\frac{P_{\star}/m_{\star}}{3000 \text{ km s}^{-1}} \right) \left(\frac{\sigma_{\text{T}}}{10 \text{ km s}^{-1}} \right)^{-1}. \quad (31)$$

A third useful expression for η can be obtained using equations (20) and (30):

$$\eta_{\text{turb}} = \frac{\mathcal{F}'}{2Q_{\text{turb}} \phi} f_{\text{out}} \left(\frac{P_{\star}}{m_{\star}} \right) (f_{\text{g}} v_{\text{c,gal}})^{-1} \quad (32)$$

$$\approx 15 \frac{\mathcal{F}'}{Q_{\text{turb}} \phi} f_{\text{out}} \left(\frac{P_{\star}/m_{\star}}{3000 \text{ km s}^{-1}} \right) \times \left(\frac{f_{\text{g}} v_{\text{c,gal}}}{100 \text{ km s}^{-1}} \right)^{-1}. \quad (33)$$

It is important to keep in mind that in the above expressions for η , f_{out} depends on the galaxy properties (\mathcal{M} and the product $Q_{\text{turb}} f_{\text{g}}$). Thus, for example, the scaling $\eta \propto (f_{\text{g}} v_{\text{c,gal}})^{-1}$ will not hold if f_{out} varies strongly with $f_{\text{g}} v_{\text{c,gal}}$.

We stress that $v_{\text{c,gal}}$ is the circular velocity of the galaxy at the effective radius, not the circular velocity of the halo. At fixed galaxy mass, $v_{\text{c,gal}}$ evolves only weakly with redshift (i.e. the Tully-Fisher relation is approximately redshift-independent; e.g. Miller et al.

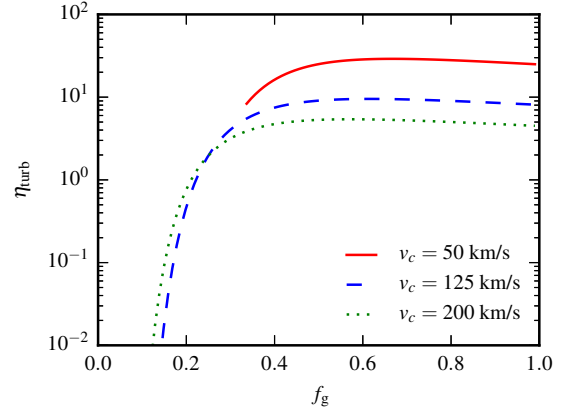


Figure 3. The mass-loading factor in the turbulent-pressure-supported regime, η_{turb} , versus the disc gas fraction, f_{g} , for different galaxy circular velocity ($v_{\text{c,gal}}$) values (see the legend). For fixed $v_{\text{c,gal}}$, η_{turb} decreases exponentially as f_{g} decreases below a critical value of ~ 0.3 because of the exponential cutoff in the outflow fraction, f_{out} (Fig. 1). This cutoff implies that once a galaxy's gas fraction decreases below the critical value of ~ 0.3 , it will no longer exhibit strong outflows. The reason for this cutoff is that for Toomre-stable discs, $\sigma_{\text{T}}/v_{\text{c,gal}} \propto f_{\text{g}}$. Thus, as the gas fraction decreases, the turbulence becomes weak, the ISM becomes relatively smooth, and a negligible fraction of the ISM is contained in sub-patches that can be blown out (i.e. that have $\Sigma_{\text{g}} < \Sigma_{\text{g}}^{\text{max}}$). (N.B. The red line is truncated at the f_{g} value below which it would no longer be turbulent pressure-supported.)

2011, 2012, 2013). In contrast, both the circular velocity at the virial radius, V_{vir} , and the maximum circular velocity of the halo, V_{max} , evolve with redshift: at fixed halo mass, both V_{vir} and V_{max} decrease with z (e.g. Somerville & Primack 1999; Bullock et al. 2001). Thus, if η is calculated using V_{vir} or V_{max} rather than the circular velocity of the galaxy, $v_{\text{c,gal}}$, at fixed virial mass (and thus approximately constant galaxy mass because the stellar-to-halo mass ratio evolves weakly with redshift; Behroozi et al. 2013; Moster et al. 2013), η will decrease with redshift. In contrast, when the circular velocity at the galaxy, $v_{\text{c,gal}}$, is used, at fixed galaxy mass, η is approximately independent of redshift (as long as we are not in the regime in which f_{out} is exponentially suppressed), as we shall see below. Thus, when implementing our model, it is crucial that the mass loading factor be calculated using the galaxy circular velocity. If a halo property must be used, it is better to use the maximum circular velocity of the halo because at fixed M_{vir} , the dependence of V_{max} on redshift is significantly weaker than that of V_{vir} (Bullock et al. 2001).

We will focus on the dependences of η_{turb} on the product $f_{\text{g}} v_{\text{c,gal}}$. Fig. 2 (3) illustrates the dependence of η_{turb} on $v_{\text{c,gal}}$ (f_{g}) for fixed values of f_{g} ($v_{\text{c,gal}}$). For sufficiently high values of f_{g} and $v_{\text{c,gal}}$, $f_{\text{out}}^{\text{turb}}$ (not shown) is approximately constant, with $f_{\text{out}}^{\text{turb}} \sim 0.5$. Thus, of order half the momentum from stellar feedback is injected into underdense regions, which are then ejected from the disc. The other half is injected into overdense regions, which are not ejected but rather ‘cycle’ over the disc scaleheight and contribute to the turbulent self-regulation of star formation. Because $f_{\text{out}}^{\text{turb}}$ is approximately constant for high values of f_{g} and $v_{\text{c,gal}}$, the predicted scalings for $f_{\text{g}} = 1$ are similar to the $\eta \propto v_{\text{c,gal}}^{-1}$ scaling expected for a momentum-driven outflow (e.g. Murray et al. 2005); the predicted scalings are slightly steeper than this because f_{out} decreases mildly with $v_{\text{c,gal}}$ even when $f_{\text{g}} = 1$. As $v_{\text{c,gal}}$ or f_{g} decrease below a critical value, $f_{\text{out}}^{\text{turb}}$ decreases ex-

ponentially, which causes η_{turb} to be significantly less than that expected from the $\eta \propto v_{c,\text{gal}}^{-1}$ scaling.

Fig. 3 is particularly useful because it clearly illustrates the transition that occurs at the critical gas fraction of ~ 0.3 . Above this critical gas fraction, the mass-loading factor for fixed $v_{c,\text{gal}}$ is approximately independent of gas fraction. However, as the gas fraction decreases from ~ 0.4 to $\lesssim 0.2$, the mass-loading factor decreases by multiple orders of magnitude. This cutoff occurs for a few reasons: first, as shown in Fig. 1, for a given Mach number, $f_{\text{out}}^{\text{turb}}$ decreases exponentially below some $Q_{\text{turb}} f_g$ value. Thus, as f_g decreases, $f_{\text{out}}^{\text{turb}}$ decreases. Furthermore, for fixed Q_{turb} , equation (20) implies that $\sigma_T \propto f_g v_{c,\text{gal}}$. Consequently, as f_g or $v_{c,\text{gal}}$ decreases, σ_T and thus (for fixed T) \mathcal{M} decrease, and Fig. 1 shows that the value of $f_{\text{out}}^{\text{turb}}$ at fixed $Q_{\text{turb}} f_g$ decreases as \mathcal{M} decreases because the gas surface density PDF becomes narrower. We stress that this cutoff is not captured in standard sub-resolution and semi-analytic models for galactic outflows and, as we shall demonstrate below, it has important implications for galaxy evolution.

4 THERMAL PRESSURE-SUPPORTED REGIME

We now consider the limit in which turbulence is weak and thus thermal pressure supports the disc against gravitational collapse. In this limit, photo-heating dominates the gas heating (Krumholz et al. 2009b; Ostriker et al. 2010). Thus, to be in this regime, the gas must not be self-shielding because once the gas is self-shielding, the heating rate will drop dramatically and the gas will collapse until it becomes turbulent-pressure-supported. For the gas to be self-shielding,

$$\Sigma_g \gtrsim 10 \text{ M}_\odot \text{ pc}^{-2} \left(\frac{Z}{Z_\odot} \right)^{-1} \equiv \Sigma_{\text{self-shield}} \quad (34)$$

(Krumholz et al. 2009a). We also require that $Q > 1$ for similar reasons. In this regime, $c_s \gg \sigma_T$. Thus,

$$Q \approx \frac{\sqrt{2} c_s \Omega}{\pi G \langle \Sigma_g \rangle} \equiv Q_{\text{th}}. \quad (35)$$

The requirement that $Q \approx Q_{\text{th}} > 1$ implies

$$\langle \Sigma_g \rangle < \frac{\sqrt{2} c_s \Omega}{\pi G} \equiv \Sigma_{Q=1}. \quad (36)$$

Assuming $T = 10^4 \text{ K}$ and thus $c_s \approx 12 \text{ km s}^{-1}$,

$$\Sigma_{Q=1} = 12 \left(\frac{\Omega}{10 \text{ Gyr}^{-1}} \right) \text{ M}_\odot \text{ pc}^{-2}. \quad (37)$$

Consequently, we consider a galaxy to be in the thermal-pressure-dominated regime if

$$\langle \Sigma_g \rangle < \min(\Sigma_{\text{self-shield}}, \Sigma_{Q=1}). \quad (38)$$

Because $\Omega \sim 10 \text{ Gyr}^{-1}$ (see Appendix B), the $Q > 1$ criterion is almost always the stricter criterion (i.e. unless $Z \gtrsim Z_\odot$, which is generally not the case for low surface-density galaxies).

Below, we will focus on galaxy-averaged properties when investigating how the mass-loading factor depends on stellar mass and redshift. The empirically based scaling relations presented in Appendix B indicate that few galaxies are in this regime in a galaxy-averaged sense (Appendix C). Thus, we do not address this limit in detail in the main text. However, our theory can also be applied to galaxies in a resolved manner, and the outskirts of galaxies can be in the thermal-pressure-supported regime. For this reason, we derive the equilibrium SFR surface density relation and mass

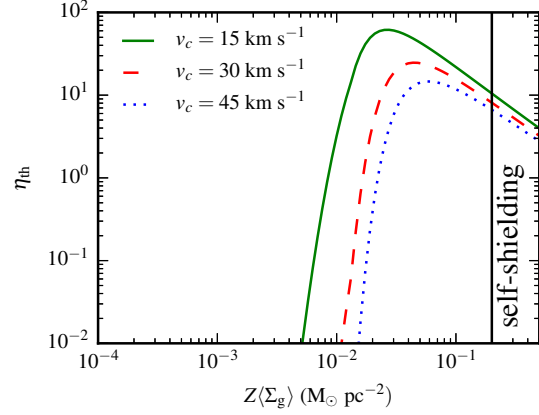


Figure 4. The mass-loading factor in the thermal-pressure-supported regime, η_{th} , versus the mean metal surface density $Z\langle\Sigma_g\rangle$ for some relevant circular velocity values (see the legend). The vertical black line denotes the self-shielding threshold; thermal-pressure-dominated galaxies lie to the left of this line by definition. Additionally, they must be Toomre-stable, which implies $\langle\Sigma_g\rangle < 12(\Omega/\text{Gyr}^{-1}) \text{ M}_\odot \text{ pc}^{-2}$. For such galaxies, η can be significant if the metal surface density is $\gtrsim 10^{-2} \text{ M}_\odot \text{ pc}^{-2}$, i.e. within one order of magnitude of the self-shielding threshold. The mass-loading factor is suppressed at lower surface densities because the momentum deposition rate per area that corresponds to the SFR surface density required to maintain self-regulation via photo-heating is too low to accelerate a significant fraction of the ISM to the escape velocity on a coherence time.

loading factor in Appendix A, and we only quote the results here. The equilibrium SFR surface density relation in this regime is

$$\dot{\Sigma}_*^{\text{th}} = \Omega Z \langle \Sigma_g \rangle \left(\frac{\langle \Sigma_g \rangle}{\Sigma_0} \right), \quad (39)$$

where

$$\Sigma_0 \approx 3 \text{ M}_\odot \text{ pc}^{-2}. \quad (40)$$

The equilibrium SFR surface density relation given by equation (39) is the equivalent of equation (16) for galaxies in the thermal-pressure-supported regime. We note that in both regimes, $\dot{\Sigma}_* \propto \langle \Sigma_g \rangle^2$, but in the thermal-pressure-supported regime, there is an additional dependence on the product ΩZ . The mass-loading factor is

$$\eta_{\text{th}} = 15 f_{\text{out}} \left(\frac{Z}{Z_\odot} \right)^{-1} \left(\frac{\langle \Sigma_g \rangle}{10 \text{ M}_\odot \text{ pc}^{-2}} \right)^{-1}, \quad (41)$$

where $f_{\text{out}}^{\text{th}} \sim 1$ for $Z\langle\Sigma_g\rangle/v_{c,\text{gal}} \gtrsim 10^{-2} \text{ M}_\odot \text{ pc}^{-2} \text{ km}^{-1} \text{ s}$ and is exponentially suppressed for $Z\langle\Sigma_g\rangle/v_{c,\text{gal}} \lesssim 2 \times 10^{-3} \text{ M}_\odot \text{ pc}^{-2} \text{ km}^{-1} \text{ s}$ (Fig. A1). Equation (41) can be approximated as

$$\eta_{\text{th}} \approx 15 \left(\frac{Z}{Z_\odot} \right)^{-1} \left(\frac{\langle \Sigma_g \rangle}{10 \text{ M}_\odot \text{ pc}^{-2}} \right)^{-1} \times \exp \left(\frac{-v_{c,\text{gal}}/Z\langle\Sigma_g\rangle}{500 \text{ km s}^{-1} \text{ M}_\odot^{-1} \text{ pc}^2} \right). \quad (42)$$

Fig. 4 shows η_{th} versus $Z\langle\Sigma_g\rangle$ for $v_{c,\text{gal}} = 15, 30$ and 45 km s^{-1} . The black vertical line indicates the self-shielding threshold; for a patch to be in the thermal-pressure-dominated regime, it must have $Z\langle\Sigma_g\rangle$ less than this limit. When a galaxy/patch is near the self-shielding limit, $f_{\text{out}}^{\text{th}} \sim 0.5$, whereas for $Z\langle\Sigma_g\rangle \lesssim 10^{-2} \text{ M}_\odot \text{ pc}^{-2}$, $f_{\text{out}}^{\text{th}} \lesssim 10^{-3}$. This indicates that there is a ‘sweet spot’, $Z\langle\Sigma_g\rangle \sim 0.1 - 1 \Sigma_{\text{self-shield}}$, in which a galaxy can both be supported by thermal pressure and exhibit

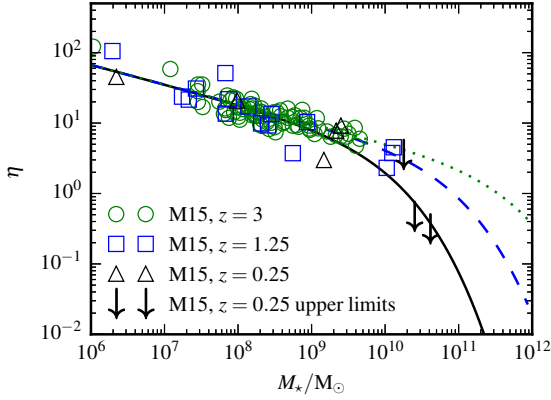


Figure 5. The mass-loading factor, η , versus stellar mass, M_* , at $z = 0.25$ (solid black), 1.25 (dashed blue), and 3 (dotted green). The mass-loading factor values for the FIRE simulations (Muratov et al. 2015) are indicated by the open symbols; the arrows denote upper limits for massive galaxies at $z = 0.25$. We have assumed that the order-unity parameter ϕ/\mathcal{F}' in equation (21) is 0.7, as this yields the best agreement with the simulation results. In massive galaxies, outflows are significantly suppressed at low redshift because their gas fractions decrease below the critical value at which the outflow fraction decreases exponentially (see Fig. 3). The reason for this cutoff is that the turbulent velocity dispersion, σ_T , required to provide vertical pressure support decreases with the gas fraction. When $\sigma_T/v_{c,\text{gal}}$ becomes too low, the amount of mass in sufficiently underdense patches becomes negligible. In contrast, outflows are driven effectively in low-mass galaxies ($M_* \lesssim 10^{10} M_\odot$) at all redshifts.

strong outflows. Because $\eta_{\text{th}} \propto f_{\text{out}}^{\text{th}} (Z \langle \Sigma_g \rangle)^{-1}$, η_{th} is maximal for patches with $Z \langle \Sigma_g \rangle \sim 0.1 \Sigma_{\text{self-shield}}$.

5 DEPENDENCE OF THE MASS-LOADING FACTOR ON STELLAR MASS AND REDSHIFT

For comparison with simulations and observations, we wish to investigate how the mass-loading factor predicted by our model depends on stellar mass and redshift. To do so, we need to know how the disc-averaged gas fraction and metallicity, the effective radius, and the circular velocity and orbital frequency at the effective radius scale with galaxy mass and redshift. It is not our purpose here to predict these quantities a priori. Thus, we will for now simply adopt empirically based fitting functions to interpolate between the observations at different redshifts. The relevant fitting functions for f_g , $v_{c,\text{gal}}$, Z , and R_e , from which scaling relations for Ω , $\langle \Sigma_g \rangle$ and σ_T are derived, are presented and plotted as a function of galaxy mass and redshift for reference in Appendix B. Because we rely on various empirically based scaling relations, the $\eta(M_*, z)$ relation that we present is by no means an ab initio prediction of our model. For this reason, those interested in implementing our model in simulations or SAMs should ideally not use the $\eta(M_*, z)$ relation but rather the physical scalings presented above (see Section 7 for details); nevertheless, we will provide a fitting function for $\eta(M_*, z)$ below.

Our assumed scaling relations imply that based on their global properties, all galaxies are expected to be turbulent-pressure-supported (see Appendix C). Only galaxies that have $\langle \Sigma_g \rangle \lesssim 10 M_\odot \text{ pc}^{-2}$, and thus lie below the empirically based $\langle \Sigma_g \rangle(M_*, z)$ relation plotted in Fig. C1, can be globally supported by thermal pressure. We thus explore how the mass loading factor

depends on stellar mass under the assumption that all galaxies are in the turbulent-pressure-supported regime. By combining equations (9), (27), (33), (B2), and (B1) and assuming an ISM temperature T , we can calculate the dependence of f_{out} and η on M_* and z . The resulting relations are presented in Fig. 5, which shows η versus M_* for $z = 0.25, 1.25$ and 3. We overplot the mass-loading factors for the FIRE simulations (Muratov et al. 2015) at the same redshifts as our model predictions. Note that the black arrows denote upper limits: as discussed by Muratov et al. (2015), galaxies in the FIRE simulations with $M_* \gtrsim 10^{10} M_\odot$ exhibit negligible mass outflow rates at $z \lesssim 1$. Note that for this plot only, we assume that the order-unity parameter $\phi/\mathcal{F}' = 0.7$ because of the few near-unity values that we tried, this gave the best agreement with the simulation results.

At high redshift, outflows are driven effectively for all M_* values. At $z = 3$, the mass-loading factor varies from ~ 70 at $M_* = 10^6 M_\odot$ to ~ 0.5 at $M_* = 10^{12} M_\odot$. For high-mass ($M_* \gtrsim 10^{10} M_\odot$) galaxies, as the redshift decreases, f_{out} and thus η decrease significantly. For $M_* \sim 10^{11} M_\odot$, η decreases by almost two orders of magnitude from $z = 3$ to $z = 0.25$. This decrease in η occurs because the gas fractions of massive galaxies decrease below the critical value at which f_{out} decreases exponentially (see Fig. 3). In contrast, in low-mass ($M_* \lesssim 10^9 M_\odot$) galaxies, η is high and approximately redshift-independent at all redshifts because these galaxies are sufficiently gas-rich even at $z = 0$.

For galaxies with $M_* \lesssim 10^{10} M_\odot$, the redshift evolution in the $\eta - M_*$ relation is weak. The reason is as follows: recall that $\eta_{\text{turb}} \propto f_{\text{out}} (f_g v_{c,\text{gal}})^{-1}$. The galaxy circular velocity (unlike the halo circular velocity) at fixed M_* is independent of redshift. The outflow fraction depends only weakly on the gas fraction as long as $f_g \gtrsim 0.3$ (which holds for these galaxies according to our assumed empirical relation), and the decrease in f_{out} with decreasing f_g is approximately canceled by the f_g^{-1} term. Thus, for galaxies with $M_* \lesssim 10^{10} M_\odot$, η scales as $\sim v_{c,\text{gal}}^{-1}$ with a normalization that is approximately independent of redshift.

The agreement between our predictions and the simulation results of Muratov et al. (2015) is impressive, especially given the simplicity of our model. In particular, a novel feature of our model is that it explains the suppression of outflows in massive galaxies at low redshift. This cutoff occurs because at low redshift, the gas fraction and thus mean gas surface density of massive galaxies decreases considerably. Consequently, the turbulent velocity expected from self-regulation decreases, and thus both Σ_g^{max} and the Mach number decrease. The fraction of the ISM that can be accelerated to the escape velocity on a dynamical time becomes negligible, and outflows are suppressed. We discuss the implications of this suppression below.

6 IMPLICATIONS FOR GALAXY EVOLUTION

We have demonstrated that our model predicts that the fiducial scaling $\eta \propto v_{c,\text{gal}}^{-1}$ will not hold for all star-forming galaxies because in our model, $\eta \propto f_{\text{out}} (Q f_g v_{c,\text{gal}})^{-1} \propto f_{\text{out}} \sigma_T^{-1}$. Thus, even if we assume that $Q = 1$ (which, as we discuss below, is a simplification), the $\eta \propto v_{c,\text{gal}}^{-1}$ scaling can be altered by variations in f_g (or equivalently σ_T) and f_{out} (which is determined by the values of Q , f_g , $v_{c,\text{gal}}$, and the diffuse ISM temperature). Consequently, models that assume a fixed $\eta \propto v_{c,\text{gal}}^{-1}$ relation (or, more generally, any model that assumes that η depends on a single global property, such as $v_{c,\text{gal}}$) may miss some important physical effects and artificially

reduce the dispersion in galaxy properties because variations in f_g at fixed $v_{c,\text{gal}}$ will directly lead to variations in η at fixed $v_{c,\text{gal}}$.

For example, suppose that a galaxy's gas fraction is temporarily lower than the quasi-equilibrium value. This could occur because of the stochastic nature of gas accretion from the intergalactic medium (e.g. Kereš & Hernquist 2009) or because the galaxy is in a post-burst state and its gas fraction has not returned to the steady-state value set by the balance of inflow and outflow. In standard models, the galaxy's mass-loading factor would remain approximately constant (assuming that $v_{c,\text{gal}}$ is approximately constant), so its outflow rate would decrease by the same factor as its SFR. Thus, the galaxy's gas content would continue to be depleted by star formation and outflows at a rate of $(1 + \eta)\dot{M}_*$ and would need an inflow rate greater than this value in order for its gas fraction to become high again. In contrast, in our model, if the gas fraction becomes sufficiently low ($f_g \lesssim 0.3$), the mass-loading factor is exponentially suppressed, and the depletion rate becomes equal to the SFR alone. Thus, as long as the inflow rate is greater than the SFR, the gas fraction will increase until the galaxy re-enters the high-outflow regime. The difference between these two depletion/required infall rates can be dramatic in $M_* \lesssim 10^{10} M_\odot$ galaxies, for which $\eta \gg 1$. This example illustrates that assuming a pure $\eta \propto v_{c,\text{gal}}^{-1}$ scaling without accounting for the cutoff that we demonstrate can artificially prevent low-mass galaxies from accumulating fresh gas and artificially suppress the variability of star formation.

The behavior can also differ in periods in which the gas surface density has been driven higher than the equilibrium value, e.g. because of an interaction. As the ISM is compressed, the SFR and thus outflow rate will increase. Assuming $\eta \propto v_{c,\text{gal}}^{-1}$ and $\dot{\Sigma}_* \propto \langle \Sigma_g \rangle^2$, for fixed $v_{c,\text{gal}}$, the mass outflow rate surface density scales as $\dot{\Sigma}_{\text{out}} \propto \langle \Sigma_g \rangle^2$. However, our model predicts that in both regimes, all else being equal, $\eta \propto f_{\text{out}} \langle \Sigma_g \rangle^{-1}$. f_{out} increases with $\langle \Sigma_g \rangle$, but this increase is weak if the galaxy already has high f_{out} (i.e. if Σ_g^{max} is not in the low- Σ_g tail of the surface density PDF). Suppose that this is the case and thus f_{out} is approximately constant (otherwise, arguments similar to those in the previous paragraph apply). Then, $\dot{\Sigma}_{\text{out}} \propto \langle \Sigma_g \rangle^{-1}$. Consequently, models that assume fixed $\eta \propto v_{c,\text{gal}}^{-1}$ scalings will tend to have greater outflow rates in starbursts than predicted by our model. These stronger outflow rates would result in artificial suppression of starbursts in such models. This effect may partially explain why large-volume cosmological simulations such as Illustris (Vogelsberger et al. 2014) do not exhibit strong starbursts (Sparre et al. 2015b), whereas galaxies in the FIRE simulations have SFRs that can vary by multiple orders of magnitude on 100-Myr timescales (Hopkins et al. 2014; Muratov et al. 2015; Sparre et al. 2015a), although resolution is another crucial difference between these two types of simulations. We note that suppression of starbursts is especially undesirable because they are critical for making realistic bulges (Hopkins et al. 2008, 2009a,c).

Moreover, as mentioned above, our model predicts that massive galaxies transition from being highly turbulent, clumpy discs that exhibit strong outflows at high redshift to well-ordered discs characterised by weak or non-existent outflows at low redshift because their gas fractions decrease below a critical value of ~ 0.3 . Suppose that the product Qf_g (or equivalently $\sigma_T/v_{c,\text{gal}}$) decreases below the critical value such that f_{out} is exponentially suppressed. The subsequent evolution depends critically on the gas inflow rate: if the gas inflow rate is greater than the SFR, the galaxy will accumulate gas (because $\eta \sim 0$), Qf_g will increase above the critical value, the galaxy will reenter the quasi-equilibrium state, and η will return to the equilibrium value. Thus, at high redshift, when

gas inflow rates are high, the quasi-equilibrium can be maintained, and galaxy evolution should be characterized by bursts of star formation (because of stochasticity in the inflow rate and mergers) and strong outflows. However, if the gas supply is insufficient to drive Qf_g back above the critical value, then the galaxy will enter a steady mode of star formation in which $\eta \sim 0$ and $\sigma_T/v_{c,\text{gal}} \ll 1$. The results of Muratov et al. (2015) indicate that galaxies with $M_* \gtrsim 10^{10} M_\odot$ transition to this regime by $z = 0$, whereas lower-mass galaxies remain in the high- η regime. This transition is potentially critical for the ability to form a thin, cold molecular (and hence young stellar) disc. In many SAMs and cosmological simulations, it is challenging to suppress early star formation, as is necessary to form disc galaxies without overly massive bulges, without destroying discs and over-suppressing star formation at $z \sim 0$ (e.g. Torrey et al. 2014; White et al. 2015). The outflow model that we present here provides a natural mechanism to address this problem, and the results of the FIRE simulations support this explanation.

We have argued that galaxies self-regulate to maintain a quasi-equilibrium state in which $Q \sim 1$ globally. The reader may object that this is inconsistent with observations of 'clumpy' galaxies at $z \sim 2$ (e.g. Genzel et al. 2011). However, we stress that this does not mean that all regions of a galaxy have $Q \sim 1$, and in fact, our model relies on overdense sub-patches of a galaxy having $Q < 1$; these patches would correspond to the observed massive star-forming clumps. Patches with $Q < 1$ collapse, form stars, and inject momentum into the surrounding ISM, thereby maintaining a global Q of order unity. Even if it is possible for galaxies to have $Q < 1$ globally, and thus be (temporarily) globally unstable, our model can be applied because we have retained the Q dependences in all expressions. Because f_{out} depends on the product Qf_g , a galaxy with global $Q = Q_1 < 1$ and gas fraction $f_g = f_{g,1}$ will have the same f_{out} as a galaxy with $Q = 1$ and gas fraction $f_g = Q_1 f_{g,1}$. For fixed f_{out} , f_g , and $v_{c,\text{gal}}$, $\eta \propto Q^{-1}$. If Qf_g is sufficiently high that f_{out} is approximately constant, a galaxy with global $Q < 1$ would have a greater outflow rates than a stable galaxy with the same f_g and $v_{c,\text{gal}}$ values, which would tend to drive the unstable galaxy back toward stability. However, if the global Q is low enough that Qf_g is less than the critical value at which f_{out} is exponentially cutoff, outflows will be suppressed, and the galaxy will unstably fragment until the gas surface density is reduced by star formation to the value required to achieve $Q = 1$. Whether the galaxy will again exhibit strong outflows will depend on the subsequent evolution of Qf_g .

It is clear that our model predictions should differ from those of the types of models currently employed in large-volume cosmological simulations and SAMs. Thus, it would be very interesting to implement our model in a cosmological simulation or SAM to investigate e.g. the implications of the cutoff discussed above. For this reason, we will now outline how one could do so.

7 HOW TO IMPLEMENT THE MODEL IN SIMULATIONS OR SEMI-ANALYTIC MODELS

As discussed above, our model can be applied to both entire galaxies and to sub-regions of galaxies, provided that the size of the sub-region is greater than the disc scaleheight. Given that state-of-the-art cosmological simulations do not resolve disc scaleheights, it would be natural to apply our model to individual resolution elements in such simulations. In SAMs, one could apply it either to individual galaxies or in annuli; the latter approach would capture potentially important effects such as variations in f_g with radius

that were ignored in the above analysis. To calculate the mass loading factor for a given galaxy, resolution element or annulus, one should proceed as follows.

(i) Depending on whether the entire galaxy or a region (i.e. resolution element or annulus) is considered, use the global or local values for Ω and Z to calculate the global or local values for $\Sigma_{Q=1}$ and $\Sigma_{\text{self-shield}}$ using equations (37) and (34), respectively.

(ii) If the value of $\langle \Sigma_g \rangle$ is less than both the $\Sigma_{Q=1}$ and $\Sigma_{\text{self-shield}}$ values, the galaxy/resolution element/annulus is in the thermal-pressure-supported regime. The mass-loading factor can then be calculated using equations (A10), (A16), (9), (10), (11) and (41). Alternatively, the approximate relation given in equation (42) can be employed.

(iii) Otherwise, the galaxy/resolution element/annulus is supported by turbulent pressure. Equations (23), (27), (9), (10), (11) and (33) can then be used to calculate the mass-loading factor.

Although we advocate using the method presented above for calculating the mass-loading factor, the scalings of η with the products $f_g v_{c,\text{gal}}$ and $f_g M_*$, including the cutoff, can be approximately captured using the following fitting functions:

$$\eta \approx 15 \left(\frac{f_g v_{c,\text{gal}}}{100 \text{ km s}^{-1}} \right)^{-1} \exp \left(\frac{-0.75}{f_g} \right) \quad (43)$$

$$\approx 14 \left(\frac{f_g M_*}{10^{10} M_\odot} \right)^{-0.23} \exp \left(\frac{-0.75}{f_g} \right). \quad (44)$$

8 CONCLUSIONS

We have presented an analytic model for how stellar feedback simultaneously regulates star formation and drives outflows in a turbulent ISM. The model is based on two fundamental assumptions: (1) star formation is self-regulating: at high surface density, the momentum input from star formation drives turbulence and supports the disc against gravitational collapse; at low surface density, when turbulence is subdominant, photo-heating stabilizes the disc. (2) Because of turbulence, the ISM exhibits a range of gas surface densities. There is a critical surface density below which gas can be accelerated to the escape velocity before the density field is ‘reset’ by turbulence. The fraction of the ISM with surface density less than this critical value is expelled in an outflow.

Our principal conclusions are as follows:

(i) In most galaxies (i.e. those with $M_* \gtrsim 10^6$ at $z = 0$, and even less massive galaxies at higher redshift), within the effective radius, turbulent pressure dominates the pressure support against gravity. For such galaxies, if the gas fraction is above the critical value of ~ 0.3 , a few tens of percent of the ISM is expelled as an outflow over an orbital time, and the outflow mass-loading factor $\eta \equiv \dot{M}_{\text{out}}/\dot{M}_*$ scales as $\eta \propto (f_g v_{c,\text{gal}})^{-1}$, where f_g is the gas fraction of the disc and $v_{c,\text{gal}}$ is the *local* circular velocity. Because at fixed redshift, galaxy gas fractions decrease with stellar mass, this scaling is slightly steeper than that expected for a momentum-driven outflow, $\eta \propto v_{c,\text{gal}}^{-1}$. When the gas fraction (or equivalently $\sqrt{2}\sigma_T/v_{c,\text{gal}}$, where σ_T is the turbulent velocity dispersion) is less than the critical value of ~ 0.3 , η is significantly less than expected from the $\eta \propto (f_g v_{c,\text{gal}})^{-1}$ scaling. The reason for this suppression is that when the turbulent velocity dispersion is low relative to the circular velocity, only patches with surface densities significantly less than the mean can be blown out. However, because of the low $\sigma_T/v_{c,\text{gal}}$, the ISM is relatively smooth, and a negligible fraction

of the ISM mass is contained in patches with surface density less than the critical value. The cutoff can be approximated using the fitting functions that we present in equations (43) and (44).

(ii) In the low- Σ_g outskirts of galaxies and in galaxies that have unusually low $\langle \Sigma_g \rangle$, thermal pressure provides the dominant support against gravity. In this regime, photo-heating from star formation rather than momentum deposition from stellar feedback maintains equilibrium. To be in this regime, a galaxy or patch of ISM must both be non-self-shielding and have $Q > 1$. Outflows can be driven effectively when the mean metal surface density is at least one-tenth the self-shielding limit, with $\eta \propto (Z \langle \Sigma_g \rangle)^{-1}$. Below this value, the mass-loading factor is exponentially suppressed.

(iii) Because low-mass galaxies are relatively gas-rich (and thus turbulent, assuming that they self-regulate to $Q \sim 1$) at all redshifts, they should exhibit mass-loading factors that are high (e.g. $\eta \sim 20$ for $M_* \sim 10^8 M_\odot$) and approximately redshift-independent at fixed stellar mass. This redshift independence occurs because the mass-loading factor depends on the galaxy circular velocity, not the halo circular velocity. Thus, models that use the halo circular velocity to calculate η , as has been often done in SAMs and cosmological simulations, will introduce redshift evolution in the $\eta - M_*$ relation that is inconsistent with our theory.

(iv) In massive galaxies ($M_* \gtrsim 10^{10} M_\odot$), outflows are suppressed at low redshift because the gas fraction, and thus turbulent velocity dispersion, of such galaxies decreases to values ($f_g \lesssim 0.3$) for which the outflow fraction decreases exponentially. For $M_* \approx 10^{11} M_\odot$ galaxies, the mass-loading factor decreases by almost two orders of magnitude from $z = 3$ to $z = 0$.

(v) We predict that this suppression of outflows is necessary for the emergence of steadily star-forming, stable, thin molecular gas (and thus young stellar) discs. Because the critical gas fraction is ~ 0.3 , only moderately massive, low-redshift galaxies can form such discs. Galaxies in which outflows are not suppressed should be characterised by cycles of starbursts, outflows, and quenched periods. This prediction is supported by the results of the FIRE simulations (Hopkins et al. 2014; Muratov et al. 2015; Sparre et al. 2015a).

(vi) The mass-loading factors predicted by our model depend on additional properties besides $v_{c,\text{gal}}$. Thus, we expect galaxies to exhibit variations in η at fixed $v_{c,\text{gal}}$; such variations are excluded by construction in the models currently assumed in large-volume cosmological simulations and SAMs.

The simple analytic model presented here is attractive because it provides a potential physical explanation for the behaviour of outflows observed in state-of-the-art simulations that explicitly model stellar feedback (Muratov et al. 2015). However, one must confirm that the various assumptions in the model hold and that further predictions of the model (e.g. weak turbulence in massive galaxies at low redshift) are borne out by the simulations; this is one avenue for future work. Moreover, it will be of interest to incorporate the predicted mass-loading factor scalings in cosmological simulations and SAMs.

ACKNOWLEDGEMENTS

We thank Lee Armus, Benham Darvish, Claude-André Faucher-Giguère, Tim Heckman, Andrey Kravtsov, Crystal Martin, Sasha Muratov, Eve Ostriker, Joel Primack, and Rachel Somerville for useful discussions, Sasha Muratov for providing data from Muratov et al. (2015) in electronic form, and Andrey

Kravtsov for noting a typo. We also thank the reviewer for a constructive report that helped improve the quality of the manuscript. CCH is grateful to the Gordon and Betty Moore Foundation for financial support, and he is especially grateful to Emmett Hayward for motivating rapid completion of the manuscript by his impending arrival, Tara Hayward for enabling his arrival, and Lori Diebold for facilitating both the completion of the manuscript and the arrival of Emmett. Support for PFH was provided by an Alfred P. Sloan Research Fellowship, NASA ATP Grant NNX14AH35G, and NSF Collaborative Research Grant #1411920 and CAREER grant #1455342. This work was supported in part by National Science Foundation Grant No. PHYS-1066293 and the hospitality of the Aspen Center for Physics, and it benefitted greatly from CCH's participation in the 2015 ACP Summer Program "The Physics of Accretion and Feedback in the Circum-Galactic Medium", the BIRS-CMO workshop "Computing the Universe: At the Intersection of Computer Science and Cosmology", and the KITP program "The Cold Universe." This research has made use of NASA's Astrophysics Data System Bibliographic Services.

REFERENCES

- Agertz O., Kravtsov A. V., 2015a, *ApJ*, 804, 18
 Agertz O., Kravtsov A. V., 2015b, *ArXiv e-prints*, arXiv:1509.00853
 Agertz O., Kravtsov A. V., Leitner S. N., Gnedin N. Y., 2013, *ApJ*, 770, 25
 Akiyama M., Minowa Y., Kobayashi N., Ohta K., Ando M., Iwata I., 2008, *ApJS*, 175, 1
 Anglés-Alcázar D., Davé R., Özel F., Oppenheimer B. D., 2014, *ApJ*, 782, 84
 Balogh M. L., Pearce F. R., Bower R. G., Kay S. T., 2001, *MNRAS*, 326, 1228
 Barden M. et al., 2005, *ApJ*, 635, 959
 Behroozi P. S., Wechsler R. H., Conroy C., 2013, *ApJ*, 770, 57
 Bell E. F., de Jong R. S., 2000, *MNRAS*, 312, 497
 Bell E. F., de Jong R. S., 2001, *ApJ*, 550, 212
 Benson A. J., 2014, *MNRAS*, 444, 2599
 Benson A. J., Bower R. G., Frenk C. S., Lacey C. G., Baugh C. M., Cole S., 2003, *ApJ*, 599, 38
 Bigiel F., Leroy A., Walter F., Brinks E., de Blok W. J. G., Madore B., Thornley M. D., 2008, *AJ*, 136, 2846
 Bigiel F. et al., 2011, *ApJ*, 730, L13
 Blanchard A., Valls-Gabaud D., Mamon G. A., 1992, *A&A*, 264, 365
 Bogdán Á. et al., 2015, *ApJ*, 804, 72
 Booth C. M., Agertz O., Kravtsov A. V., Gnedin N. Y., 2013, *ApJ*, 777, L16
 Bordoloi R. et al., 2011, *ApJ*, 743, 10
 Bouché N., Hohensee W., Vargas R., Kacprzak G. G., Martin C. L., Cooke J., Churchill C. W., 2012, *MNRAS*, 426, 801
 Bournaud F., Elmegreen B. G., Teyssier R., Block D. L., Puerari I., 2010, *MNRAS*, 409, 1088
 Bullock J. S., Kolatt T. S., Sigad Y., Somerville R. S., Kravtsov A. V., Klypin A. A., Primack J. R., Dekel A., 2001, *MNRAS*, 321, 559
 Bullock J. S., Kravtsov A. V., Weinberg D. H., 2000, *ApJ*, 539, 517
 Burbidge E. M., Burbidge G. R., Rubin V. C., 1964, *ApJ*, 140, 942
 Calura F., Jimenez R., Panter B., Matteucci F., Heavens A. F., 2008, *ApJ*, 682, 252
 Cantó J., Raga A. C., Rodríguez L. F., 2000, *ApJ*, 536, 896
 Chabrier G., 2003, *PASP*, 115, 763
 Chisholm J., Tremonti C. A., Leitherer C., Chen Y., Wofford A., Lundgren B., 2014, *ArXiv e-prints*, arXiv:1412.2139
 Cioffi D. F., McKee C. F., Bertschinger E., 1988, *ApJ*, 334, 252
 Cole S., 1991, *ApJ*, 367, 45
 Conroy C., Wechsler R. H., 2009, *ApJ*, 696, 620
 Cox T. J., Di Matteo T., Hernquist L., Hopkins P. F., Robertson B., Springel V., 2006, *ApJ*, 643, 692
 Crain R. A. et al., 2015, *MNRAS*, 450, 1937
 Cresci G. et al., 2009, *ApJ*, 697, 115
 Croton D. J. et al., 2006, *MNRAS*, 365, 11
 Dalla Vecchia C., Schaye J., 2008, *MNRAS*, 387, 1431
 Dalla Vecchia C., Schaye J., 2012, *MNRAS*, 426, 140
 Davé R., Finlator K., Oppenheimer B. D., 2011a, *MNRAS*, 416, 1354
 Davé R., Katz N., Oppenheimer B. D., Kollmeier J. A., Weinberg D. H., 2013, *MNRAS*, 434, 2645
 Davé R., Oppenheimer B. D., Finlator K., 2011b, *MNRAS*, 415, 11
 Davé R., Oppenheimer B. D., Katz N., Kollmeier J. A., Weinberg D. H., 2010, *MNRAS*, 408, 2051
 Dekel A., Silk J., 1986, *ApJ*, 303, 39
 Diamond-Stanic A. M., Moustakas J., Tremonti C. A., Coil A. L., Hickox R. C., Robaina A. R., Rudnick G. H., Sell P. H., 2012, *ApJ*, 755, L26
 Dubois Y., Teyssier R., 2008, *A&A*, 477, 79
 Erb D. K., 2008, *ApJ*, 674, 151
 Erb D. K., Shapley A. E., Pettini M., Steidel C. C., Reddy N. A., Adelberger K. L., 2006a, *ApJ*, 644, 813
 Erb D. K., Steidel C. C., Shapley A. E., Pettini M., Reddy N. A., Adelberger K. L., 2006b, *ApJ*, 646, 107
 Faucher-Giguère C.-A., Quataert E., Hopkins P. F., 2013, *MNRAS*, 433, 1970
 Federrath C., Roman-Duval J., Klessen R. S., Schmidt W., Mac Low M.-M., 2010, *A&A*, 512, A81
 Ferguson H. C. et al., 2004, *ApJ*, 600, L107
 Ford A. B., Davé R., Oppenheimer B. D., Katz N., Kollmeier J. A., Thompson R., Weinberg D. H., 2014, *MNRAS*, 444, 1260
 Ford A. B., Oppenheimer B. D., Davé R., Katz N., Kollmeier J. A., Weinberg D. H., 2013, *MNRAS*, 432, 89
 Ford A. B. et al., 2015, *ArXiv e-prints*, arXiv:1503.02084
 Förster Schreiber N. M. et al., 2009, *ApJ*, 706, 1364
 Genel S. et al., 2014, *MNRAS*, 445, 175
 Genzel R. et al., 2011, *ApJ*, 733, 101
 Girichidis P. et al., 2016, *ApJ*, 816, L19
 Governato F. et al., 2010, *Nature*, 463, 203
 Governato F., Willman B., Mayer L., Brooks A., Stinson G., Valenzuela O., Wadsley J., Quinn T., 2007, *MNRAS*, 374, 1479
 Governato F. et al., 2012, *MNRAS*, 422, 1231
 Guo Q., White S., Angulo R. E., Henriques B., Lemson G., Boylan-Kolchin M., Thomas P., Short C., 2013, *MNRAS*, 428, 1351
 Guo Q. et al., 2011, *MNRAS*, 413, 101
 Hanasz M., Lesch H., Naab T., Gawryszczak A., Kowalik K., Wóltański D., 2013, *ApJ*, 777, L38
 Hayward C. C., Narayanan D., Kereš D., Jonsson P., Hopkins P. F., Cox T. J., Hernquist L., 2013, *MNRAS*, 428, 2529
 Heckman T. M., Alexandroff R. M., Borthakur S., Overzier R., Leitherer C., 2015, *ApJ*, 809, 147
 Heckman T. M., Armus L., Miley G. K., 1990, *ApJS*, 74, 833
 Heckman T. M., Lehnert M. D., Strickland D. K., Armus L., 2000, *ApJS*, 129, 493
 Hill A. S., Joing M. R., Mac Low M.-M., Benjamin R. A., Haffner L. M., Klingenberg C., Waagan K., 2012, *ApJ*, 750, 104
 Hirschmann M. et al., 2013, *MNRAS*, 436, 2929
 Hoefl M., Yepes G., Gottlöber S., Springel V., 2006, *MNRAS*, 371, 401
 Hopkins P. F., Cox T. J., Dutta S. N., Hernquist L., Kormendy J., Lauer T. R., 2009a, *ApJS*, 181, 135
 Hopkins P. F., Hernquist L., Cox T. J., Dutta S. N., Rothberg B., 2008, *ApJ*, 679, 156
 Hopkins P. F., Hernquist L., Cox T. J., Keres D., Wuyts S., 2009b, *ApJ*, 691, 1424
 Hopkins P. F., Kereš D., Murray N., Hernquist L., Narayanan D., Hayward C. C., 2013, *MNRAS*, 433, 78
 Hopkins P. F., Kereš D., Oñorbe J., Faucher-Giguère C.-A., Quataert E., Murray N., Bullock J. S., 2014, *MNRAS*, 445, 581
 Hopkins P. F., Lauer T. R., Cox T. J., Hernquist L., Kormendy J., 2009c, *ApJS*, 181, 486
 Hopkins P. F., Quataert E., Murray N., 2012a, *MNRAS*, 421, 3522
 Hopkins P. F., Quataert E., Murray N., 2012b, *MNRAS*, 421, 3488

- Hopkins P. F., Younger J. D., Hayward C. C., Narayanan D., Hernquist L., 2010, *MNRAS*, 402, 1693
- Katz N., Weinberg D. H., Hernquist L., 1996, *ApJS*, 105, 19
- Kennicutt, Jr. R. C., 1998, *ApJ*, 498, 541
- Kereš D., Hernquist L., 2009, *ApJ*, 700, L1
- Kereš D., Katz N., Fardal M., Davé R., Weinberg D. H., 2009, *MNRAS*, 395, 160
- Kereš D., Katz N., Weinberg D. H., Davé R., 2005, *MNRAS*, 363, 2
- Kim C.-G., Kim W.-T., Ostriker E. C., 2011, *ApJ*, 743, 25
- Kim C.-G., Ostriker E. C., Kim W.-T., 2013, *ApJ*, 776, 1
- Konstandin L., Federrath C., Klessen R. S., Schmidt W., 2012a, *Journal of Fluid Mechanics*, 692, 183
- Konstandin L., Girichidis P., Federrath C., Klessen R. S., 2012b, *ApJ*, 761, 149
- Konstandin L., Schmidt W., Girichidis P., Peters T., Shetty R., Klessen R. S., 2015, *ArXiv e-prints*, arXiv:1506.03834
- Kroupa P., 2001, *MNRAS*, 322, 231
- Krumholz M. R., Dekel A., McKee C. F., 2012, *ApJ*, 745, 69
- Krumholz M. R., McKee C. F., 2005, *ApJ*, 630, 250
- Krumholz M. R., McKee C. F., Tumlinson J., 2009a, *ApJ*, 693, 216
- Krumholz M. R., McKee C. F., Tumlinson J., 2009b, *ApJ*, 699, 850
- Larson R. B., 1974, *MNRAS*, 169, 229
- Le Brun A. M. C., McCarthy I. G., Schaye J., Ponman T. J., 2014, *MNRAS*, 441, 1270
- Leitherer C., Chandar R., Tremonti C. A., Wofford A., Schaerer D., 2013, *ApJ*, 772, 120
- Leitherer C. et al., 1999, *ApJS*, 123, 3
- Leroy A. K. et al., 2015, *ArXiv e-prints*, arXiv:1509.02932
- Leroy A. K. et al., 2013, *AJ*, 146, 19
- Li M., Ostriker J. P., Cen R., Bryan G. L., Naab T., 2015, *ApJ*, 814, 4
- Lu Y., Blanc G. A., Benson A., 2015, *ApJ*, 808, 129
- Lu Y., Mo H. J., Lu Z., Katz N., Weinberg M. D., 2014, *MNRAS*, 443, 1252
- Lynds C. R., Sandage A. R., 1963, *ApJ*, 137, 1005
- Mac Low M.-M., Ferrara A., 1999, *ApJ*, 513, 142
- Maiolino R. et al., 2008, *A&A*, 488, 463
- Mannucci F. et al., 2009, *MNRAS*, 398, 1915
- Martin C. L., 1996, *ApJ*, 465, 680
- Martin C. L., 1998, *ApJ*, 506, 222
- Martin C. L., 1999, *ApJ*, 513, 156
- Martin C. L., 2005, *ApJ*, 621, 227
- Martin C. L., 2006, *ApJ*, 647, 222
- Martin C. L., Shapley A. E., Coil A. L., Kornei K. A., Bundy K., Weiner B. J., Noeske K. G., Schiminovich D., 2012, *ApJ*, 760, 127
- Martizzi D., Faucher-Giguère C.-A., Quataert E., 2015, *MNRAS*, 450, 504
- Mathews W. G., Baker J. C., 1971, *ApJ*, 170, 241
- McGaugh S. S., 2005, *ApJ*, 632, 859
- Miller S. H., Bundy K., Sullivan M., Ellis R. S., Treu T., 2011, *ApJ*, 741, 115
- Miller S. H., Ellis R. S., Sullivan M., Bundy K., Newman A. B., Treu T., 2012, *ApJ*, 753, 74
- Miller S. H., Sullivan M., Ellis R. S., 2013, *ApJ*, 762, L11
- Mitra S., Davé R., Finlator K., 2015, *MNRAS*, 452, 1184
- Moster B. P., Naab T., White S. D. M., 2013, *MNRAS*, 428, 3121
- Muratov A. L., Keres D., Faucher-Giguère C.-A., Hopkins P. F., Quataert E., Murray N., 2015, *ArXiv e-prints*, arXiv:1501.03155
- Murray N., 2011, *ApJ*, 729, 133
- Murray N., Ménard B., Thompson T. A., 2011, *ApJ*, 735, 66
- Murray N., Quataert E., Thompson T. A., 2005, *ApJ*, 618, 569
- Murray N., Quataert E., Thompson T. A., 2010, *ApJ*, 709, 191
- Navarro J. F., White S. D. M., 1993, *MNRAS*, 265, 271
- Okamoto T., Frenk C. S., Jenkins A., Theuns T., 2010, *MNRAS*, 406, 208
- Okamoto T., Gao L., Theuns T., 2008, *MNRAS*, 390, 920
- Oppenheimer B. D., Davé R., 2006, *MNRAS*, 373, 1265
- Oppenheimer B. D., Davé R., 2008, *MNRAS*, 387, 577
- Oppenheimer B. D., Davé R., 2009, *MNRAS*, 395, 1875
- Oppenheimer B. D., Davé R., Katz N., Kollmeier J. A., Weinberg D. H., 2012, *MNRAS*, 420, 829
- Oppenheimer B. D., Davé R., Kereš D., Fardal M., Katz N., Kollmeier J. A., Weinberg D. H., 2010, *MNRAS*, 406, 2325
- Ostriker E. C., McKee C. F., Leroy A. K., 2010, *ApJ*, 721, 975
- Ostriker E. C., Shetty R., 2011, *ApJ*, 731, 41
- Ostriker E. C., Stone J. M., Gammie C. F., 2001, *ApJ*, 546, 980
- Puchwein E., Springel V., 2013, *MNRAS*, 428, 2966
- Puech M. et al., 2008, *A&A*, 484, 173
- Ravindranath S. et al., 2004, *ApJ*, 604, L9
- Robertson B. E., Kravtsov A. V., 2008, *ApJ*, 680, 1083
- Salem M., Bryan G. L., 2014, *MNRAS*, 437, 3312
- Salem M., Bryan G. L., Hummels C., 2014, *ApJ*, 797, L18
- Savaglio S. et al., 2005, *ApJ*, 635, 260
- Schaye J. et al., 2015, *MNRAS*, 446, 521
- Schaye J. et al., 2010, *MNRAS*, 402, 1536
- Schmidt M., 1959, *ApJ*, 129, 243
- Scoville N., 2003, *Journal of Korean Astronomical Society*, 36, 167
- Sedov L. I., 1959, *Similarity and Dimensional Methods in Mechanics*
- Shapley A. E., Coil A. L., Ma C.-P., Bundy K., 2005, *ApJ*, 635, 1006
- Shetty R., Ostriker E. C., 2008, *ApJ*, 684, 978
- Shetty R., Ostriker E. C., 2012, *ApJ*, 754, 2
- Somerville R. S., Davé R., 2014, *ArXiv e-prints*, arXiv:1412.2712
- Somerville R. S., Hopkins P. F., Cox T. J., Robertson B. E., Hernquist L., 2008, *MNRAS*, 391, 481
- Somerville R. S., Primack J. R., 1999, *MNRAS*, 310, 1087
- Sparre M., Hayward C. C., Feldmann R., Faucher-Giguère C.-A., Muratov A. L., Kereš D., Hopkins P. F., 2015a, *ArXiv e-prints*, arXiv:1510.03869
- Sparre M. et al., 2015b, *MNRAS*, 447, 3548
- Springel V., Hernquist L., 2003, *MNRAS*, 339, 289
- Steidel C. C., Erb D. K., Shapley A. E., Pettini M., Reddy N., Bogosavljević M., Rudie G. C., Rakic O., 2010, *ApJ*, 717, 289
- Stinson G., Seth A., Katz N., Wadsley J., Governato F., Quinn T., 2006, *MNRAS*, 373, 1074
- Stinson G. S., Brook C., Macciò A. V., Wadsley J., Quinn T. R., Couchman H. M. P., 2013, *MNRAS*, 428, 129
- Strickland D. K., Stevens I. R., 2000, *MNRAS*, 314, 511
- Taylor G., 1950, *Royal Society of London Proceedings Series A*, 201, 159
- Thacker R. J., Couchman H. M. P., 2000, *ApJ*, 545, 728
- Thompson T. A., Krumholz M. R., 2016, *MNRAS*, 455, 334
- Thompson T. A., Quataert E., Murray N., 2005, *ApJ*, 630, 167
- Thornton K., Gaudlitz M., Janka H.-T., Steinmetz M., 1998, *ApJ*, 500, 95
- Thoul A. A., Weinberg D. H., 1996, *ApJ*, 465, 608
- Toft S. et al., 2007, *ApJ*, 671, 285
- Toomre A., 1964, *ApJ*, 139, 1217
- Torrey P., Vogelsberger M., Genel S., Sijacki D., Springel V., Hernquist L., 2014, *MNRAS*, 438, 1985
- Trujillo I. et al., 2004, *ApJ*, 604, 521
- Tully R. B., Fisher J. R., 1977, *A&A*, 54, 661
- Uhlig M., Pfrommer C., Sharma M., Nath B. B., Enßlin T. A., Springel V., 2012, *MNRAS*, 423, 2374
- Vázquez-Semadeni E., García N., 2001, *ApJ*, 557, 727
- Veilleux S., Cecil G., Bland-Hawthorn J., 2005, *ARA&A*, 43, 769
- Vogelsberger M., Genel S., Sijacki D., Torrey P., Springel V., Hernquist L., 2013, *MNRAS*, 436, 3031
- Vogelsberger M. et al., 2014, *MNRAS*, 444, 1518
- Wada K., Norman C. A., 2001, *ApJ*, 547, 172
- Weiner B. J. et al., 2009, *ApJ*, 692, 187
- White C. E., Somerville R. S., Ferguson H. C., 2015, *ApJ*, 799, 201
- White S. D. M., Frenk C. S., 1991, *ApJ*, 379, 52
- White S. D. M., Rees M. J., 1978, *MNRAS*, 183, 341
- Zhang D., Thompson T. A., Murray N., Quataert E., 2014, *ApJ*, 784, 93

APPENDIX A: DERIVATIONS FOR THE THERMAL-PRESSURE-DOMINATED REGIME

Here, we derive the equilibrium surface density and mass-loading factor relations for the thermal-pressure-dominated regime (equations 39 and 41 in the main text).

A1 The equilibrium SFR surface density relation

In this regime, thermal pressure supports the disc against gravity. Thus, the equilibrium SFR will be set by the requirement that photo-heating from star formation balances cooling.⁷ For photoionization, which should dominate the heating, the heating rate per unit area is

$$\frac{\dot{E}_{\text{heat}}}{A} = \frac{\beta L}{A} = \beta \epsilon c^2 \dot{\Sigma}_*, \quad (\text{A1})$$

where $\beta \sim 0.1$ is the fraction of the stellar luminosity that is emitted as ionizing photons (Leitherer et al. 1999) and $\epsilon \sim 4 \times 10^{-4}$ is the ratio of the energy emitted over the life of a star to its rest-mass energy. For other forms of heating, only the prefactor β differs. The cooling rate per unit area is

$$\frac{\dot{E}_{\text{cool}}}{A} = \frac{\Lambda n_e n_i V}{A} \approx \Lambda \mu^{-1} \langle \Sigma_g \rangle Z n_g, \quad (\text{A2})$$

where n_e , n_i , and n_g are the electron, ion, and total gas number densities, respectively, V is the volume, Z is the metallicity, and $\Lambda \sim 10^{-22}$ ergs s⁻¹ cm³ is the net cooling rate (e.g. Robertson & Kravtsov 2008). Setting equations (A1) and (A2) equal, we have

$$\dot{\Sigma}_* = \frac{\Lambda}{\mu \beta \epsilon c^2} Z n_g \langle \Sigma_g \rangle \equiv \dot{\Sigma}_*^{\text{th}}. \quad (\text{A3})$$

Using $n_g = \rho_g / \mu$, $\rho = \langle \Sigma_g \rangle / 2h$ (where h is the disc scale height) and $h = \sqrt{c_s^2 + \sigma_T^2} / \sqrt{2} \Omega \approx c_s / \sqrt{2} \Omega$ (because we assume that thermal pressure dominates the pressure support in this regime), we have

$$n_g = \frac{\langle \Sigma_g \rangle \Omega}{\sqrt{2} \mu c_s}. \quad (\text{A4})$$

Combining equations (A3) and (A4), it follows that

$$\dot{\Sigma}_*^{\text{th}} = \frac{\Lambda}{\sqrt{2} \mu^2 \beta \epsilon c^2 c_s} Z \langle \Sigma_g \rangle^2 \Omega \quad (\text{A5})$$

$$= \Omega Z \langle \Sigma_g \rangle \left(\frac{\langle \Sigma_g \rangle}{\Sigma_0} \right), \quad (\text{A6})$$

where we have defined

$$\Sigma_0 \equiv \frac{\sqrt{2} \mu^2 \beta \epsilon c^2 c_s}{\Lambda} \approx 3 \text{ M}_\odot \text{ pc}^{-2}, \quad (\text{A7})$$

assuming $T = 10^4 \text{ K}$ and thus $c_s \approx 12 \text{ km s}^{-1}$. The equilibrium SFR surface density relation given by equation (A6) is the equivalent of equation (16) for galaxies in the thermal-pressure-supported regime. We note that in both regimes, $\dot{\Sigma}_* \propto \langle \Sigma_g \rangle^2$, but in the thermal-pressure-supported regime, there is an additional dependence on Z (and also Ω , but the variation in this quantity with stellar mass and redshift is much less than that in Z).

A2 Mass-loading factor

With the equilibrium SFR surface density relation in hand, we can now calculate the surface density below which gas can be blown out by momentum deposition from stellar feedback on a coherence time. Again, as discussed in Section 2, we stress that we are assuming that the outflows are momentum-driven in this regime because the mass-loading factor for energy-driven outflows is low, our assumed P_*/m_* value implicitly includes the energy-conserving phase of SN remnants, and most material that is at sufficiently low surface density that SN remnants can break out of the disc while still in the energy-conserving phase will also satisfy the criterion for being blown out in a momentum-driven outflow. Using equation (5), we have

$$\Sigma_g^{\text{max}} = \frac{1}{\sqrt{2}} \left(\frac{P_*}{m_*} \right) v_{\text{c,gal}}^{-1} Z \langle \Sigma_g \rangle \left(\frac{\langle \Sigma_g \rangle}{\Sigma_0} \right) \equiv \Sigma_{g,\text{th}}^{\text{max}}. \quad (\text{A8})$$

⁷ The metagalactic background radiation can also photoheat the gas, but this component is expected to be important only in the far outer disc regions of galaxies, where $\Sigma_g \ll 1 \text{ M}_\odot \text{ pc}^{-2}$ (see Ostriker et al. 2010 for a detailed discussion).

Consequently,

$$x_{\text{out}} = \ln \left[\frac{1}{\sqrt{2}} \left(\frac{P_*}{m_*} \right) v_{\text{c,gal}}^{-1} Z \left(\frac{\langle \Sigma_g \rangle}{\Sigma_0} \right) \right] \equiv x_{\text{out}}^{\text{th}} \quad (\text{A9})$$

$$= \ln \left[14 \left(\frac{P_*/m_*}{3000 \text{ km s}^{-1}} \right) \left(\frac{Z}{Z_\odot} \right) \times \left(\frac{v_{\text{c,gal}}}{\text{km s}^{-1}} \right)^{-1} \left(\frac{\langle \Sigma_g \rangle}{\text{M}_\odot \text{ pc}^{-2}} \right) \right], \quad (\text{A10})$$

where we have used $Z_\odot = 0.02$. Combining equations (12) and (A6) yields

$$\eta = f_{\text{out}} Z^{-1} \left(\frac{\langle \Sigma_g \rangle}{\Sigma_0} \right)^{-1} \equiv \eta_{\text{th}} \quad (\text{A11})$$

$$= 15 f_{\text{out}} \left(\frac{Z}{Z_\odot} \right)^{-1} \left(\frac{\langle \Sigma_g \rangle}{10 \text{ M}_\odot \text{ pc}^{-2}} \right)^{-1}. \quad (\text{A12})$$

We note that η is inversely proportional to the optical depth through the disc, $\tau \propto Z \langle \Sigma_g \rangle$.

To solve for the outflow fraction, f_{out} , we need to determine the Mach number, \mathcal{M} . We assume that stellar feedback drives the turbulence, although turbulent pressure does not support the disc against gravity in this regime. Then, to calculate the turbulent velocity dispersion, we equate the rate at which momentum is injected by stellar feedback (equation 4) to the rate at which turbulence dissipates momentum, $\dot{\Sigma}_{\text{P,disp}} \sim \langle \Sigma_g \rangle \sigma_T \Omega$. This yields

$$\sigma_T \sim \left(\frac{P_*}{m_*} \right) \frac{\dot{\Sigma}_*}{\langle \Sigma_g \rangle \Omega}. \quad (\text{A13})$$

Using the equilibrium SFR surface density relation for this regime (equation A6), we have

$$\sigma_T \sim \left(\frac{P_*}{m_*} \right) \frac{Z \langle \Sigma_g \rangle}{\Sigma_0} \quad (\text{A14})$$

$$= 20 \text{ km s}^{-1} \left(\frac{P_*/m_*}{3000 \text{ km s}^{-1}} \right) \left(\frac{Z}{0.1 Z_\odot} \right) \times \left(\frac{\langle \Sigma_g \rangle}{10 \text{ M}_\odot \text{ pc}^{-2}} \right). \quad (\text{A15})$$

Thus,

$$\mathcal{M} \sim 1.7 \left(\frac{P_*/m_*}{3000 \text{ km s}^{-1}} \right) \left(\frac{Z}{0.1 Z_\odot} \right) \left(\frac{\langle \Sigma_g \rangle}{10 \text{ M}_\odot \text{ pc}^{-2}} \right) \times \left(\frac{\mu}{0.6} \right)^{1/2} \left(\frac{T}{10^4 \text{ K}} \right)^{-1/2} \equiv \mathcal{M}_{\text{th}}. \quad (\text{A16})$$

To calculate the outflow fraction, we perform the integral specified in equation (9) using $x_{\text{out}} = x_{\text{out}}^{\text{th}}$ (equation A10).⁸ Fig. A1 shows the outflow fraction $f_{\text{out}}^{\text{th}}$ versus $Z \langle \Sigma_g \rangle / v_{\text{c,gal}}$ for Mach numbers of 1.1, 5, 10, and 20. In all cases, $f_{\text{out}}^{\text{th}}$ asymptotes to unity for $Z \langle \Sigma_g \rangle / v_{\text{c,gal}} \gtrsim 10^{-2} \text{ M}_\odot \text{ pc}^{-2} \text{ km}^{-1} \text{ s}$, and it declines steeply below $\sim 10^{-3} \text{ M}_\odot \text{ pc}^{-2} \text{ km}^{-1} \text{ s}$.

APPENDIX B: GALAXY SCALING RELATIONS

To predict η as a function of M_* and z , we require parameterizations for the dependence of the circular velocity at the effective radius ($v_{\text{c,gal}}$), the disc gas fraction [$f_g \equiv M_g / (M_* + M_g)$], the effective radius (R_e) and the metallicity (Z) on M_* and z . For $v_{\text{c,gal}}(M_*)$, we assume that the stellar Tully & Fisher (1977) relation of Bell & de Jong (2001),

$$v_{\text{c,gal}} = 147 \left(\frac{M_*}{10^{10} \text{ M}_\odot} \right)^{0.23} \text{ km s}^{-1}, \quad (\text{B1})$$

⁸ Note that when the turbulence becomes trans-sonic, $\alpha = 3.7$ should be used in equation (11); see TK14 for discussion.

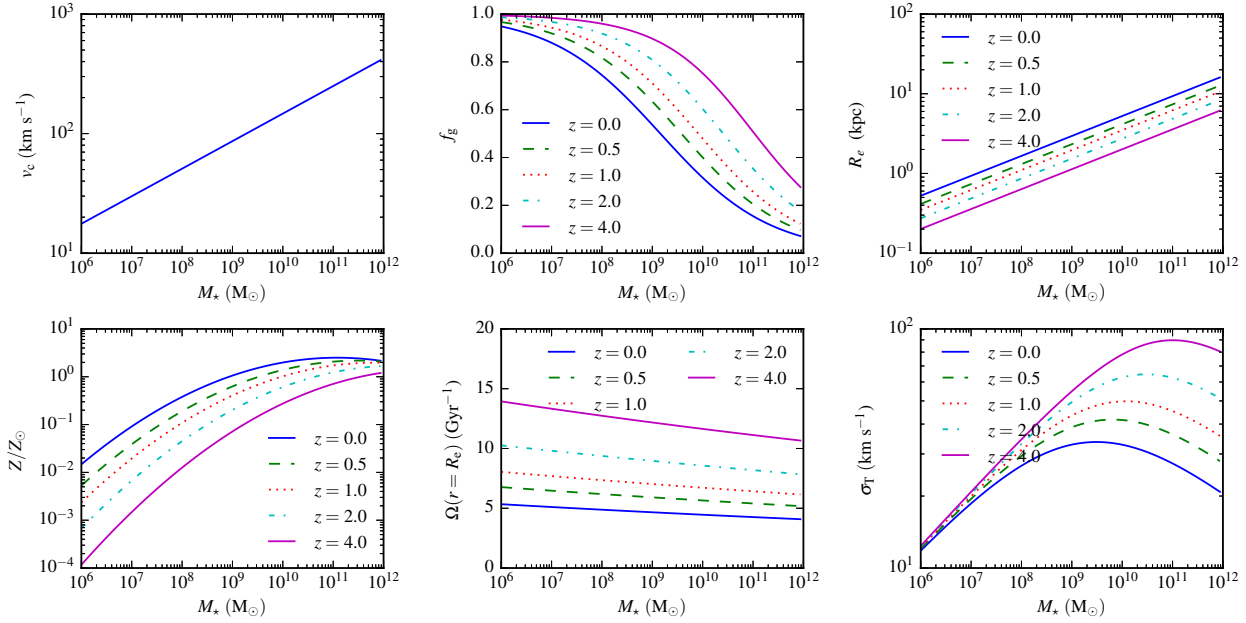


Figure B1. Empirically based dependences of galaxy circular velocity (*top left*), gas fraction (*top middle*), effective radius (*top right*), metallicity (*bottom left*), orbital frequency at the effective radius ($\Omega_{R_e} \approx v_{c,\text{gal}}/2\pi R_e$; *bottom middle*) and turbulent velocity dispersion ($\sigma_T \approx f_g v_{c,\text{gal}}/\sqrt{2}$ for $Q_{\text{turb}} = 1$; *bottom right*) on stellar mass at various redshifts. The *circular velocity* increases with stellar mass in a redshift-independent manner. *Gas fraction*: at fixed z , f_g decreases with M_* . At fixed M_* , f_g increases with z . *Effective radius* increases (decreases) weakly with stellar mass (redshift). *Metallicity* increases (decreases) with stellar mass (redshift). *Orbital frequency*: for the redshift range $z = 0 - 4$, Ω_{R_e} varies by less than a factor of 3 over 6 orders of magnitude in stellar mass. It decreases (increases) very weakly with stellar mass (redshift). *Turbulent velocity dispersion*: for $M_* \lesssim 10^8 M_\odot$, $\sigma_T \propto v_{c,\text{gal}}$ because $f_g \sim 1$ at all redshifts. At higher stellar masses, the increase in $v_{c,\text{gal}}$ with stellar mass is counteracted by the decrease in f_g , thereby causing the value of σ_T at fixed z to decrease above some M_* value. At fixed M_* , σ_T increases with z because galaxies are more gas-rich at high redshift.

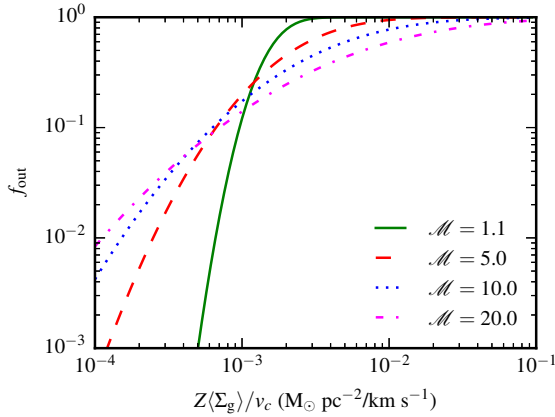


Figure A1. The fraction of the ISM blown out per dynamical time in the thermal-pressure-dominated regime, $f_{\text{out}}^{\text{th}}$, versus $Z(\Sigma_g)/v_{c,\text{gal}}$ for different Mach numbers (see the legend). When $Z(\Sigma_g)/v_{c,\text{gal}}$ (i.e. the mean metal surface density divided by the circular velocity) is $\gtrsim 10^{-2} M_\odot \text{pc}^{-2} \text{km}^{-1} \text{s}$, $f_{\text{out}}^{\text{th}} \sim 1$, which means that the entire ISM can be blown out on a dynamical time. At $Z(\Sigma_g)/v_{c,\text{gal}} \lesssim 10^{-3} M_\odot \text{pc}^{-2} \text{km}^{-1} \text{s}$, $f_{\text{out}}^{\text{th}}$ is exponentially suppressed because the momentum deposition rate per area that corresponds to the SFR surface density required to maintain self-regulation via photo-heating is too low to accelerate a significant fraction of the ISM to the escape velocity on a coherence time.

where we have divided the Bell & de Jong (2001) masses by 1.7 to convert to a Kroupa (2001) initial mass function, holds at all redshifts. The relation is plotted in the upper-left panel of Fig. B1. This specific (redshift-

independent) parameterization is reasonable from $z = 0$ to at least $z \sim 1.7$ (Miller et al. 2011, 2012, 2013).

For f_g , we use the relation from Hopkins et al. (2009b, 2010):

$$f_g(M_*, z) = f_0 \left[1 - \tau(z) \left(1 - f_0^{3/2} \right) \right]^{-2/3}, \quad (\text{B2})$$

where $\tau(z)$ is the fractional lookback time to redshift z . This relation was obtained by fitting a theoretically motivated functional form (Kereš et al. 2005, 2009) to a compilation of observations (Bell & de Jong 2000; McGaugh 2005; Shapley et al. 2005; Erb et al. 2006b; Erb 2008; Calura et al. 2008; Puech et al. 2008; Cresci et al. 2009; Förster Schreiber et al. 2009; Mannucci et al. 2009). For convenience, we show f_g versus M_* in the upper-middle panel of Fig. B1.

For the effective radius, we use the scaling relation from Hopkins et al. (2010),

$$R_e(M_*, z) = R_e(M_*, z=0) (1+z)^{-0.6}, \quad (\text{B3})$$

which is based on a compilation of observations (Trujillo et al. 2004; Ravindranath et al. 2004; Ferguson et al. 2004; Barden et al. 2005; Toft et al. 2007; Akiyama et al. 2008). This relation is shown in the upper-right panel of Fig. B1.

For Z , we use the $Z(M_*, z)$ relation presented in [Hayward et al. \(2013\)](#),⁹

$$\begin{aligned} \log \left(\frac{Z(M_*, z)}{Z_\odot} \right) &= -8.69 + 9.09(1+z)^{-0.017} \\ &- 0.0864 \left[\log \left(\frac{M_*}{M_\odot} \right) \right. \\ &- \left. 11.07(1+z)^{0.094} \right]^2, \end{aligned} \quad (\text{B4})$$

(B5)

which is based on observations from [Savaglio et al. \(2005\)](#), [Erb et al. \(2006a\)](#) and [Maiolino et al. \(2008\)](#). For reference, the relation is plotted in the bottom-left panel of [Fig. B1](#).

It is interesting to consider some of the scalings that result from the above scalings. The bottom-middle panel of [Fig. B1](#) shows the orbital frequency at the effective radius, $\Omega_{R_e} \approx v_{c,\text{gal}}/2\pi R_e$, versus M_* for various redshifts. At fixed z , $R_e \propto M_*^{0.25}$, and $v_{c,\text{gal}} \propto M_*^{0.26}$ at all redshifts. Thus, at fixed z , Ω_{R_e} is approximately constant, and it increases mildly from $\sim 5 \text{ Gyr}^{-1}$ at $z = 0$ to $\sim 10 - 15 \text{ Gyr}^{-1}$ at $z = 4$.

The bottom-right panel of [Fig. B1](#) shows how the turbulent velocity dispersion (equation 20) depends on M_* at different redshifts; we assume $Q_{\text{turb}} = 1$. σ_T ranges from $\sim 10 \text{ km s}^{-1}$ at $M_* \sim 10^6 M_\odot$ to $\sim 100 \text{ km s}^{-1}$ in $M_* \sim 10^{11} M_\odot$ discs at $z = 4$. For $M_* \lesssim 10^8 M_\odot$, $f_g \sim 1$ at all redshifts. Thus, $\sigma_T \approx v_{c,\text{gal}}/\sqrt{2}$, which is related to the stellar mass by the assumed Tully-Fisher relation. At higher stellar masses, σ_T is approximately constant at fixed redshift because the increase in $v_{c,\text{gal}}$ with stellar mass is offset by the decrease in f_g . For fixed $M_* \gtrsim 10^8 M_\odot$, σ_T increases with z because f_g increases with z ; i.e. high-redshift massive disc galaxies are much more turbulent than their local counterparts.

APPENDIX C: ARE GALAXIES SUPPORTED BY TURBULENT OR THERMAL PRESSURE?

We now use the scaling relations presented above to determine as a function of stellar mass and redshift whether galaxies are supported by turbulent or thermal pressure (on average within the effective radius).

The gas surface density can be calculated using $\langle \Sigma_g \rangle = \pi R_e^2 f_g / (1 - f_g) M_*$. The left panel of [Fig. C1](#) shows $\langle \Sigma_g \rangle$ versus M_* for various redshifts. At fixed z , $\langle \Sigma_g \rangle$ increases weakly with M_* (i.e. less than one order of magnitude over 8 orders of magnitude in stellar mass) because the increase in $\langle \Sigma_g \rangle$ that would result from the increase in total galaxy mass if all other quantities were held fixed is almost completely mitigated by the decrease in f_g and increase in R_e with M_* . At fixed M_* , $\langle \Sigma_g \rangle$ increases with z because f_g increases and R_e decreases. At $z = 0$, $\langle \Sigma_g \rangle \sim 20 - 100 M_\odot \text{ pc}^{-2}$, whereas at $z = 4$, $\langle \Sigma_g \rangle \sim 1000 - 3000 M_\odot \text{ pc}^{-2}$.

To determine whether a galaxy is self-shielding, we require $Z(\Sigma_g)$, which can be calculated using the scaling relations for f_g , R_e , and Z . The right panel of [Fig. C1](#) shows the resulting relationship between $Z(\Sigma_g)$ and M_* at various redshifts. The solid black horizontal line indicates $Z(\Sigma_g) < 0.2 M_\odot \text{ pc}^{-2}$, the surface density above which the galaxy is self-shielding. At fixed z , $Z(\Sigma_g)$ increases approximately linearly with M_* for $M_* \lesssim 10^8 M_\odot$, and the relation flattens at higher stellar masses. At the low-mass end, $Z(\Sigma_g)$ increases decreases mildly with increasing z because the redshift evolution in Z is stronger than that in $\langle \Sigma_g \rangle$. At the high-mass end, the opposite holds. For our present purposes, the most important feature to note is that independent of redshift, galaxies with $M_* \gtrsim 10^8 M_\odot$ are self-shielding and thus globally in the turbulent-pressure-supported regime.

In addition to not being self-shielding, a galaxy must have $Q > 1$ to be in the thermal-pressure-supported regime. Given the values for Ω shown

in the bottom-middle panel of [Fig. B1](#), $Q > 1$ (see equation 37) corresponds to $\langle \Sigma_g \rangle \lesssim 10 M_\odot \text{ pc}^{-2}$. From [Fig. C1](#), we see that, at least assuming that the extrapolations of our empirically based relations are reasonable, no galaxies have $Q_{\text{th}} > 1$. Consequently, no galaxies in equilibrium with typical properties should be globally thermal-pressure-supported. However, galaxies with lower-than-typical Σ_g values can be in the thermal-pressure-supported regime, and it is possible that the outskirts of galaxies can be in this regime even if the galaxy-averaged properties put it in the turbulent-pressure-supported regime.

⁹ In equation (12) of [Hayward et al. \(2013\)](#), the exponent of the first $(1+z)$ term should be 0.094, not 0.94. The correct value of 0.094 is stated in the text above the equation and was used in the calculations in that work.

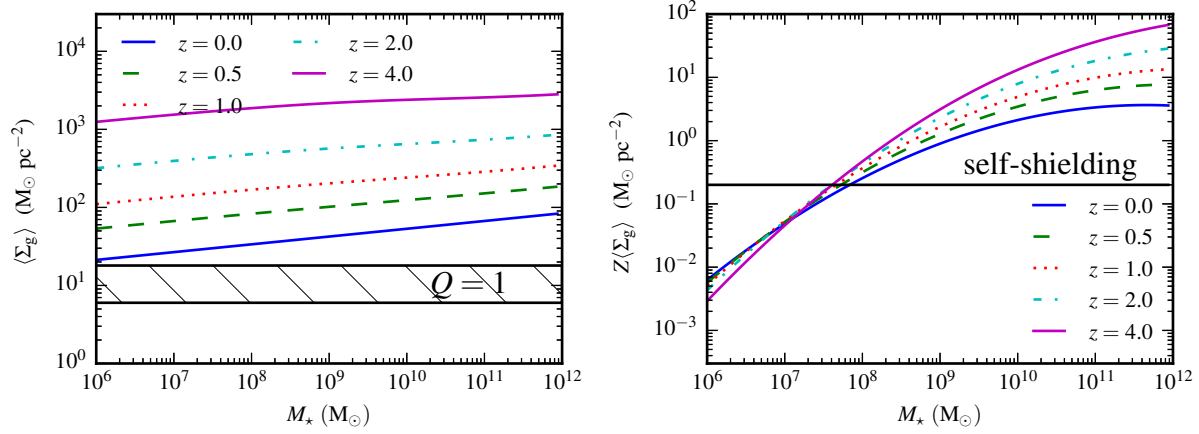


Figure C1. Mean gas (*left*) and metal (*right*) surface density versus stellar mass at various redshifts calculated using our empirically based scalings for f_g , R_e , and Z . In the *left* panel, the hatched region indicates where the thermal Toomre Q is unity (assuming $\Omega \sim 5 - 15 \text{ Gyr}^{-1}$; see equation 37). Galaxies located above this region have sufficiently high gas surface densities that they cannot be supported by thermal pressure alone. For the galaxy scaling relations that we assume, effectively all galaxies have $Q_{\text{th}} < 1$ and thus cannot be globally in the thermal-pressure-dominated regime (although the outskirts of galaxies and galaxies with lower-than-average $\langle \Sigma_g \rangle$ values can be). In the *right* panel, the black horizontal line indicates the limit above which the galaxy is self-shielding. Independent of redshift, the mean metal surface densities of $M_\star \gtrsim 10^8 \text{ M}_\odot$ galaxies are greater than the self-shielding threshold.